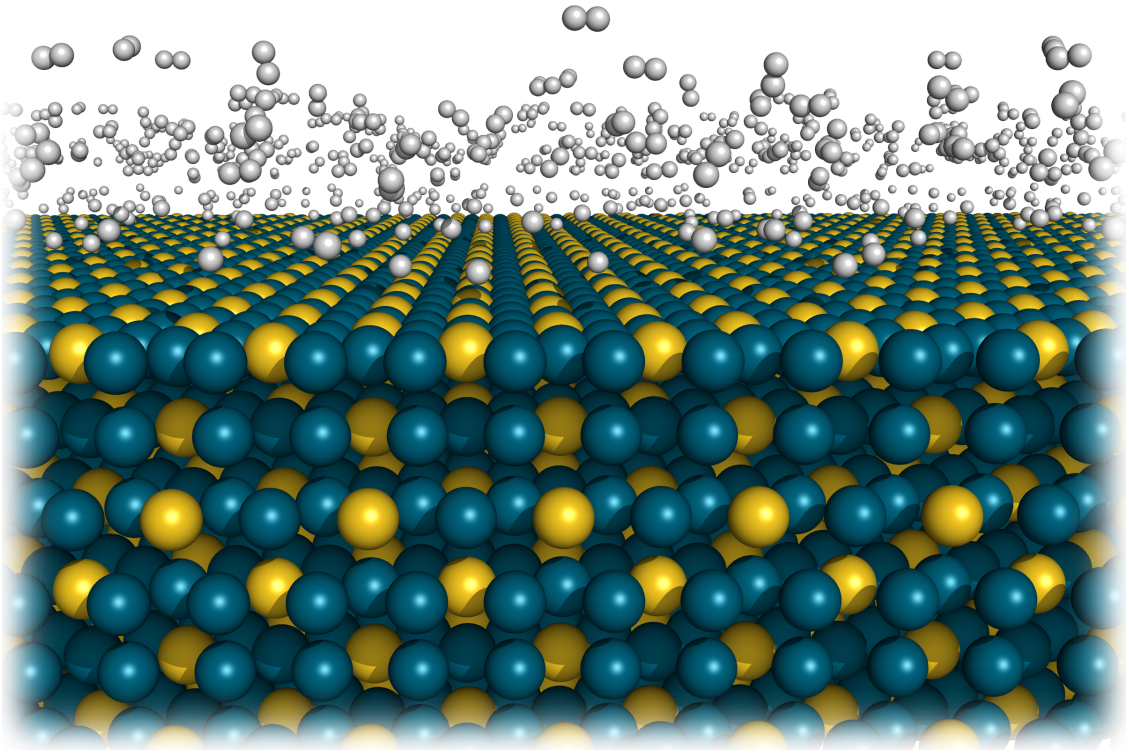
CHALMERS
UNIVERSITY OF TECHNOLOGY



Hydrogen on PdAu surfaces: Diffusion and segregation

Master's thesis in Physics and Astronomy

UNNI ENGEDAHL

Department of Physics
Division of Chemical Physics
CHALMERS UNIVERSITY OF TECHNOLOGY
Gothenburg, Sweden 2016

Master's thesis 2016

Hydrogen on PdAu surfaces: Diffusion and segregation

UNNI ENGEDAHL



CHALMERS
UNIVERSITY OF TECHNOLOGY

Department of Physics
Division of Chemical Physics
Competence Centre for Catalysis
Chalmers University of Technology
Gothenburg, Sweden 2016

Hydrogen on PdAu surfaces: Diffusion and segregation
UNNI ENGEDAHL

© UNNI ENGEDAHL, 2016.

Supervisor and examiner: Henrik Grönbeck, Department of Chemical Physics

Department of Physics
Division of Chemical Physics
Competence Centre for Catalysis
Chalmers University of Technology
SE-412 96 Gothenburg
Telephone +46 31 772 1000

Cover: Interface between a PdAu surface and an environment of hydrogen.

Typeset in LaTeX
Printed by Chalmers Reproservice
Gothenburg, Sweden 2016

Hydrogen on PdAu surfaces: Diffusion and segregation
Unni Engedahl
Department of Physics
Chalmers University of Technology

Abstract

The possibility for hydrogen to dissociate on palladium surfaces and to diffuse subsurface makes palladium interesting for hydrogen storage and membrane applications. The properties of palladium may be modified and tuned by metal alloying. It is clear that the mixing of the metals in the surface region depend on the gas phase and the operating conditions. In this thesis, Density Functional Theory (DFT) calculations have been used to investigate hydrogen adsorption on Pd_3Au surfaces and by studying the fcc(111) surface composition as a function of coverage how hydrogen may change the alloy composition in the surface layer. In addition, the effect of alloying on hydrogen subsurface diffusion have been investigated. The surface layer is composed entirely of Au in the absence of hydrogen. Increasing the hydrogen coverage favors Pd segregation to the first and the second surface layer. The segregation is induced by the strong hydrogen-palladium bond. Alloying is found to have marked effects on the diffusion of hydrogen into the bulk of the metal. The most important changes with respect to the bare Pd metal is a reduction of the surface to subsurface barrier and a slightly higher barrier for diffusion in the interior of the alloy.

Keywords: Density Functional Theory, palladium, gold, hydrogen, adsorption, storage, coverage, surface segregation, diffusion

Acknowledgements

Henrik Grönbeck, for the opportunity and all the time you put into this project!

All calculations were performed at the computer center C^{3}SE at Chalmers, with CPU time provided through a SNIC grant.

Unni Engedahl, Gothenburg, April 2016

Contents

List of Figures **xi**

List of Tables **xiii**

Preface 1

1 Introduction **3**
1.1 Objective 4

2 Quantum mechanics and atoms **5**
2.1 Electronic structure 5
2.1.1 The Hamiltonian 5
2.1.2 The Schrödinger equation 6
2.1.3 Orbitals 6
2.2 The Born-Oppenheimer approximation 8

Method 10

3 Density functional theory **13**
3.1 Hohenberg-Kohn theorems 13
3.2 The Kohn-Sham equation 14
3.2.1 Exchange-correlation approximations 15
3.2.2 Solving the Kohn-Sham equation 15
3.3 Computational implementation 16
3.4 Choice of computational parameters 16

4 Analyzing first-principles calculations **19**
4.1 Characterization 19
4.1.1 Surface stability 20
4.1.2 Adsorption energy 21
4.2 Analysis of electronic structure 21
4.2.1 Bader analysis 21
4.2.2 Local alloy composition 22
4.2.3 Density of states 22

Results **24**

5 Bulk and surface **27**
5.1 Bulk properties . . . 27
5.2 Surface structures and properties . . . 29
5.2.1 Zero-point energy . . . 31

6 Adsorption **33**
6.1 Surface structures . . . 33
6.1.1 Monoatomic surface structures . . . 33
6.1.2 The alloyed surface structures . . . 34
6.2 Bader analysis . . . 35
6.3 Local alloy composition . . . 36
6.4 Density of states . . . 37
6.4.1 Bulk and surface DOS . . . 37
6.4.2 Lattice strain, d-band center, and adsorption energy . . . 39
6.4.3 The hydrogen DOS . . . 40

7 Effects of hydrogen coverage **43**
7.1 Surface layer configurations . . . 43
7.2 Subsurface layer configurations . . . 46

8 Diffusion **49**
8.1 Pd . . . 50
8.1.1 Structural analysis . . . 51
8.2 PdAu . . . 52
8.2.1 Bare $PdAu_3$ terminated alloy surface . . . 54
8.2.2 Loaded Pd_3Au terminated alloy surface . . . 55
8.2.3 Structural analysis . . . 55

Epilogue **57**

9 Conclusion **59**
9.1 Segregation of surface metal atoms . . . 59
9.2 Diffusion of hydrogen . . . 59

10 Outlook **61**

Bibliography **63**

A Numerical values **I**

List of Figures

1.1 Selective Pd membrane 3

3.1 Convergence, pure Pd and Au bulks 17

4.1 d-band theory, effects of adsorbate interaction 23

5.1 Surfaces structures and energies 29
5.2 Surface energy vs. local alloy composition 31

6.1 Adsorption sites on a monometallic surface 33
6.2 Adsorption, surface models 34
6.3 Adsorption sites, Pd_3Au terminated alloy surface 34
6.4 Adsorption sites, Pd_2Au_2 terminated alloy surface 35
6.5 Adsorption sites, $PdAu_3$ terminated alloy surface 35
6.6 Adsorption energy vs. local alloy composition 36
6.7 DOS and d-band center: pure Pd, and Au; slab and bulk 37
6.8 DOS and d-band center, PdAu bulk 38
6.9 DOS and d-band center, alloy surfaces 38
6.10 Density of state and adsorption energy 39
6.11 DOS, adsorption on strained Pd surface 41

7.1 Loading, surface layer configurations 43
7.2 Total energy vs. coverage, surface layer 44
7.3 Total and differential adsorption energy vs. coverage, surface layer 44
7.4 Segregation vs. coverage, surface layer 45
7.5 Loading, subsurface layer configurations 46
7.6 Total energy vs. coverage, subsurface layer 46
7.7 Total and differential adsorption energy vs. coverage, subsurface layer . . . 47
7.8 Segregation vs. coverage, subsurface layer 47

8.1 Adsorption sites, monometallic bulk 49
8.2 Diffusion, Pd bulk 50
8.3 Diffusion, through Pd surface 51
8.4 Lattice strain, effect on adsorption 52
8.5 Adsorption sites, alloy bulk 53
8.6 Characteristics of diffusion, Pd3Au bulk 53
8.7 Characteristics of diffusion, bare $PdAu_3$ surface 54
8.8 Characteristics of diffusion, loaded Pd_3Au surface 55

List of Tables

5.1 Bulk properties: Pd, Au, and Pd_xAu_y 28
5.2 Charge analysis, bulk and bare surface 30

6.1 Adsorption energies, monometallic surfaces 33
6.2 Adsorption sites, Pd_3Au terminated alloy surface 34
6.3 Adsorption sites, Pd_2Au_2 terminated alloy surface 35
6.4 Adsorption sites, $PdAu_3$ terminated alloy surface 35
6.5 Charge analysis, adsorption 36

8.1 Distances, diffusion in Pd 51
8.2 Distances, diffusion in PdAu 56

A.1 Pd, strained lattice II
A.2 Interatomic distances, Pd bulk with strained lattice II
A.3 Charge analysis III
A.4 Total energies and adsorption energies vs. H coverage IV
A.5 Adsorption energies V
A.6 Diffusion barriers V
A.7 Energy differences VI

Preface

Chapter 1

Introduction

As the transport sector continues to grow there is a need for renewable, environmentally friendly, energy sources or carriers. In the search for low pollution fuel, hydrogen is a possible good option as the manufacturing process of this energy carrier is believed to have high potential of becoming environmentally friendly and cost effective. However, there are some obstacles in reaching the full potential of the gas. One application is as fuel in the low-temperature, fuel cell (Proton exchange membrane (PEM) fuel cells), where one problem is CO poisoning [1]. The catalyst, which is used on both the anode and cathode side, is made out of platinum. At low temperatures, CO adsorbs strongly on Pt and block the metal sites for the fuel cell reactions. Thus, the hydrogen that is fed into the fuel cell has to be free from CO.

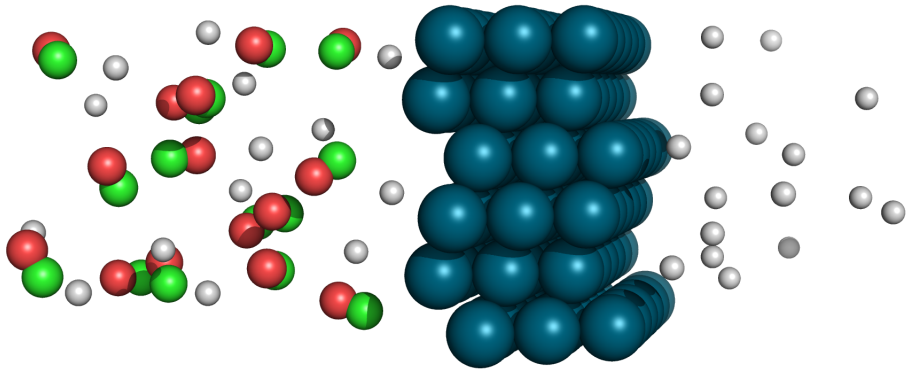


Figure 1.1: *Sketch of a selective Pd membrane. Atomic color code: Oxygen (red), carbon (green), palladium (blue), and hydrogen (white).*

There are different ways of removing CO from an H_2 gas. One way would be to selectively react CO with oxygen forming CO_2 [2]. (This reaction is difficult as also H_2 reacts with O_2 forming H_2O.) Another option is the use of thin, high permeability Pd-based membranes, through which only hydrogen is able to diffuse, seen Figure 1.1 [3]. During the loading and unloading of hydrogen in the operation of the membrane, the material continuously transforms between the alpha and beta phase of the palladium hydride. The repeated expansion and contraction of the Pd lattice causes embrittlement in the material, reducing the operational lifetime for the system [3]. If possible, one would for these membranes like to enhance both the selectivity and the durability.

Alloying Pd with a noble metal such as Au may enhance the catalytic activity and selectivity. Not only enhancing the reactivity but also pre-expanding the lattice may lead to an increased efficiency and lifetime of the membrane. As Pd is a metal known to store hydrogen; however, with a slow storage kinetics due to the diffusion barriers, alloying the metal with Au may also improve the storage capacity.

1.1 Objective

Properties of surfaces may differ from the corresponding bulk material for electronic as well as structural reasons. The structure and local composition of the surface may change as a dynamic response to the environment. This project will investigate properties of PdAu surfaces in an environment of hydrogen. As a well defined reference, Pd and PdAu in the bulk phase will also be investigated. Given a specified Pd/Au ratio, the questions that will be addressed are:

1. What is the composition of the low index PdAu surfaces?
2. What is the diffusion barriers for H in the PdAu surface?
3. What is the diffusion barriers for H in the PdAu bulk?
4. What is the composition of PdAu as a function of H coverage?

Chapter 2

Quantum mechanics and atoms

2.1 Electronic structure

The Bohr model, with its point like nucleus and electrons in stationary circular orbits, is a semi-classical description of the atom and its electrons. Despite its simplicity, the model describes many aspects of atoms correctly and these simply need to be reinterpreted when a complete quantum mechanical treatment is imposed on a system. For instance, it is Heisenberg's uncertainty principle that prevents the atom from caving in on itself, and the anti-symmetry of the fermionic wave function that gives rise to the different electronic states and orbitals. The classical model has, however, some fundamental flaws. One is that it does not obey the particle-wave duality that all matter possesses. Instead of treating the electrons as charged point masses moving around the nucleus they should be viewed as propagating wave packets and thus, described by wave functions. Taking into account the uncertainty in the electronic position, the fact that only the likelihood of an electron being at a certain place can be determined, gives the quantum mechanical probability amplitudes and the theory of orbitals emerges.

2.1.1 The Hamiltonian

To investigate and predict how a system behaves requires that the Hamiltonian is known. Being an "energy matrix", it describes all the physical interactions in the system and consequently also how the system evolves with time. The Hamiltonian is of course not the same for every system but all systems have one and the challenge is finding out what it looks like.

The fundamentals of the Hamiltonian ($\hat{H}$) are always the same; it is the sum of the kinetic ($\hat{T}$) and potential ($\hat{V}$) energy of the system:

$$\hat{H} = \hat{T} + \hat{V}. \tag{2.1}$$

For the molecular Hamiltonian, the potential energy can be further divided:

$$\hat{H} = \hat{T} + \hat{V}_{ext} + \hat{V}_{int} + E_{II} \tag{2.2}$$

The terms for a system with i electrons and I nuclei in atomic units[1] are:

$\hat{T} = -\frac{1}{2}\sum_i \nabla_i^2$	Kinetic energy operator for the electrons
$\hat{V}_{ext} = -\sum_{i,I} \frac{Z_I}{\mid \mathbf{r}_i - \mathbf{R}_I \mid}$	Potential acting on the electrons due to the nuclei
$\hat{V}_{int} = \frac{1}{2}\sum_{i \neq j} \frac{1}{\mid \mathbf{r}_i - \mathbf{r}_j \mid}$	Electron-electron interaction
E_{II}	Classical interaction between nuclei, viewed as point charges, and any other term contributing to the total energy of the system that is not related to the electrons.

Putting these pieces back together as in eq. (2.1) creates the complete Hamiltonian for a system of atoms:

$$\hat{H} = -\frac{1}{2}\sum_i \nabla_i^2 - \sum_{i,I} \frac{Z_I}{\mid \mathbf{r}_i - \mathbf{R}_I \mid} + \frac{1}{2}\sum_{i \neq j} \frac{1}{\mid \mathbf{r}_i - \mathbf{r}_j \mid} - \sum_I \frac{1}{2M_I}\nabla_I^2 + \frac{1}{2}\sum_{I \neq J} \frac{Z_I Z_J}{\mid \mathbf{R}_I - \mathbf{R}_J \mid} \quad (2.3)$$

Here the electrons are denoted by lower case letters and the nuclei, carrying charge Z and mass M, are denoted by upper case.

2.1.2 The Schrödinger equation

Given the Hamiltonian, the total energy of the system can be evaluated by solution of the Schrödinger equation. This is a wave equation that describe all non-relativistic quantum systems. For a stationary electronic state, described by the wave function $\Psi(\mathbf{r}_1, \ldots, \mathbf{r}_N)$, the many-electron time-independent Schrödinger equation is

$$\begin{aligned} \hat{H}\Psi &= \left[\hat{T} + \hat{V}_{ext} + \hat{V}_{int} + E_{II}\right]\Psi \\ &= \left[-\frac{1}{2}\sum_i \nabla_i^2 - \sum_{i,I} \frac{Z_I}{\mid \mathbf{r}_i - \mathbf{R}_I \mid} + \frac{1}{2}\sum_{i \neq j} \frac{1}{\mid \mathbf{r}_i - \mathbf{r}_j \mid} - \sum_I \frac{1}{2M_I}\nabla_I^2 + \frac{1}{2}\sum_{I \neq J} \frac{Z_I Z_J}{\mid \mathbf{R}_I - \mathbf{R}_J \mid}\right]\Psi \\ &= E\Psi \end{aligned} \quad (2.4)$$

2.1.3 Orbitals

When knowing how to mathematically describe a system, it is interesting to look at the solution of the Schrödinger equation for an atom. As the electrons "revolve" the nucleus of an atom, they do not actually move in the circular orbits as described by the Bohr model. The area given by the probability density that quantum mechanically describes the electron position, is depicted by something called orbitals. (When one also considers the electronic spin, one speaks of spin orbitals.) These orbitals are characterized by a unique set of quantum numbers (no spin-orbit interaction):

[1] $m = e = \hbar = \frac{1}{4\pi\epsilon_0} = 1$

Principal quantum number, n

Describes the energy level, or shell. It assumes integers starting at 1. Every number corresponds to a different shell, where 1 is often called K, 2 L, 3 M, and so on.

Azimuthal (or orbital) quantum number, l

Describes the subshell and gives the magnitude of the orbital angular momentum via $L^2 = \hbar^2 l(l+1)$. Assumes integer values $0, 1, 2, ..., n-1$. Each subshell is identified by a letter: 0,1,2, and 3 corresponds to s,p,d, and f.

Magnetic quantum number, m_l

Gives the specific orbital, or cloud, within each subshell and the projection of the orbital angular momentum along a given axis, $L_z = m_l\hbar$. Its values range, in integer steps, from $-l$ to l.

Spin projection quantum number, m_s

Gives the spin (intrinsic angular momentum) of the individual electrons and the projection of the spin angular momentum S along a given axis, $S_z = m_s\hbar$. Takes on the values -$s, -s+1, ..., s-1, s$ where s is the particles spin quantum number. For fermions, such as the electron, s is 1/2.

For each value of l, an electron can assume $2(2l+1)$ different states depending on the two remaining quantum numbers, m_l och m_s.

Table 2.1: *Correlation between quantum numbers.*

n	l	m_l	m_s	Name	Number of e^-
1	0	0	$-1/2, 1/2$	1s	2
2	0	0	$-1/2, 1/2$	2s	2
	1	-1,0,1	$-1/2, 1/2$	2p	6
3	0	0	$-1/2, 1/2$	3s	2
	1	-1,0,1	$-1/2, 1/2$	3p	6
	2	-2,-1,0,1,2	$-1/2, 1/2$	3d	10
					and so on

In Bohr's model, n determines the radius of each circular electron orbit. All electrons with the same n lie at the same average distance to the nucleus, in the same shell. These shells are filled successively according to their energy - lowest levels are filled first. Filling the orbitals as in a one-electron system would correspond to the order in Table 2.2. However this is not always the case.

Table 2.2: *The theoretical order in which the shells will, successively, be filled with electrons is from left to right, starting in the upper left corner.*

1s				
2s				2p
3s				3p
4s			3d	4p
5s			4d	5p
6s		4f	5d	6p
7s		5f	6d	7p
8s	5g	6f	7d	8p

To elucidate this, let's see some examples of shells filled in theoretical order:
Hydrogen (^{1}H) has the electron structure $1s^1$
Quantum numbers: $n = 1$, $m_l = 0$, $l = 0$; and 1 electron in its sole electron shell.
Gold (^{79}Au) has the structure $1s^2 2s^2 2p^6 3s^2 3p^6 4s^2 3d^{10} 4p^6 5s^2 4d^{10} 5p^6 4f^{14} 5d^{10} 6s^1$
Quantum numbers: $n = 5$, $m_l = 2$, $l = 2$; and 2, 8, 18, 32, 18, and 1 electron in its respective shells.

and one of shells not filled in theoretical order:
Palladium (^{46}Pd) has the structure $1s^2 2s^2 2p^6 3s^2 3p^6 4s^2 3d^{10} 4p^6 4d^{10}$
Quantum numbers: $n = 4$, $m_l = 3$, $l = 3$; and 2, 8, 18, and 18 electrons per shell.

For reaction and reactivity, the electron configuration in the valence region is most important. For a free Au atom this is $5d^{10}6s^1$, giving a valence charge of 11, while Pd has $4d^{10}$ for the isolated atom and close to $4d^9 5s^1$ in the condensed phase, and a charge of 10.

2.2 The Born-Oppenheimer approximation

When actually attempting to solve the Schrödinger equation for a molecular or condensed state, the problem should be simplified as far as possible. Often the first step is to apply the Born-Oppenheimer approximation. The purpose of this approximation is to reduce the degrees of freedom in the Hamiltonian of the system. As the mass of the nucleus is large compared to that of the electrons, the motions of the nucleus is on a longer time scale, making it appear stationary as compared to the motion of the electron. This "fixed nucleus" approximation is equivalent to the existence of a static external potential in which the electrons are moving. Effectively it is now possible to separate the electronic part of the wave function from the rest, arriving at a somewhat less complicated expression of the electronic Hamiltonian,

$$\hat{H} = \sum_{i=1}^{N} \left(\frac{\mathbf{p}_i^2}{2m} + V_{ext}(\mathbf{r}_j) + \frac{1}{2} \sum_{i \neq j}^{N} \frac{e^2}{\mid \mathbf{r}_i - \mathbf{r}_j \mid} \right), \tag{2.5}$$

in which the positions of the nuclei are simply parameters.

If trying to simplify the problem further the electron-electron interaction turns out to make it impossible to separate $\hat{H}$ into simpler equations of only parts of the system.

The Schödinger equation of this electronic system,

$$\hat{H}\Psi = \left[\hat{T} + \hat{V}_{ext} + \hat{U}\right]\Psi = \left[\sum_{i}^{N}\left(-\frac{\hbar^2}{2m_i}\nabla_i^2\right) + \sum_{i}^{N} V_{ext}(\mathbf{r}_i) + \sum_{i<j}^{N} U(\mathbf{r}_i, \mathbf{r}_j)\right]\Psi = E\Psi \qquad (2.6)$$

is a quantum mechanical wave function which contains, in principle, all the information about the system and in some of the simplest cases, as for instance for a square 2D potential or the hydrogen atom, eq. (2.6) is exactly solvable.

If expanding the system from one to two particles, the result is not a Schrödinger equation of two wave functions but rather that of one two-particle function. The former 3 dimensional equation becomes 6 dimensional and thus, the complexity of the equation describing the system increases rapidly with the number of particles in the system. As a consequence, when dealing with more complex systems, the Schrödinger equation becomes impossible to solve exactly.

Method

Chapter 3

Density functional theory

When investigating large, complex systems, solving the Schrödinger equation becomes an insurmountable undertaking and this is why Density Functional Theory (DFT) is applied. It provides what is needed; an approximative solution to the Schrödinger equation of a many-body system.

3.1 Hohenberg-Kohn theorems

The success of DFT is built on two fundamental theorems, both devised by Hohenberg and Kohn [4]:

1. When in an external potential, V_{ext}, the total energy of a system is a functional of the electronic density,

$$E[n(\mathbf{r})] = \int d\mathbf{r} V_{ext} n(\mathbf{r}) + F[n(\mathbf{r})]. \tag{3.1}$$

   In other words, the electron density fully determines the Hamiltonian of the many-body system. This allows for a complete and unique determination of electronic properties.

2. The energy functional of the system, E[n], can be defined to be valid for any V_{ext}, and the exact ground state of the system is determined by the global minimum value of this functional.

$$E_0 = \int d\mathbf{r} V_{ext} n_0(\mathbf{r}) + F[n_0] \tag{3.2}$$

   Or, the ground state density gives the ground state energy.

Thus, using the electron density, $n(x, y, z)$, a function of three spatial coordinates can replace the myriad of electrons in the wave function of the system. This turns the wave function into a density functional[1], reducing the number of dimensions from $3N$, $\Psi(r_1(x, y, z), \ldots, r_N(x, y, z))$, to just 3, $\Psi(n(x, y, z))$.

[1] Functional simply meaning a function ($E[n]$) of a function ($n(\mathbf{r})$).

In eq. (3.1), the right hand side is conveniently separated into two terms. The second term $F[n(\mathbf{r})]$ being the universal functional that contains the individual contributions of the kinetic energy, the classic Coulomb interaction, and the non-classical self-interaction correction but is independent of the external potential V_{ext}.

3.2 The Kohn-Sham equation

The total energy of a system of many electrons is in DFT given by [5]

$$E = T + \int d\mathbf{r} n(\mathbf{r}) V_{ext} + \frac{1}{2} \int \int d\mathbf{r} d\mathbf{r}' \frac{n(\mathbf{r}) n(\mathbf{r}')}{|\mathbf{r} - \mathbf{r}'|} + E_{xc}^{true} \tag{3.3}$$

with

$$E_{xc}^{true} = \frac{1}{2} \int \int d\mathbf{r} d\mathbf{r}' \frac{n(\mathbf{r}) n(\mathbf{r}')}{|\mathbf{r} - \mathbf{r}'|} [g(\mathbf{r} - \mathbf{r}') - 1]. \tag{3.4}$$

Here, the most difficult part of the Hohenberg-Kohn functional, the non-classical interaction between the electrons, is separated from the classical Coulomb interaction and the kinetic energy of $F[n(\mathbf{r})]$ in eq. (3.1). This non-classical interaction has two contributions and is called the exchange-correlation interaction. The exchange interaction is due to the Pauli principle, the fact that two electrons with parallel spin must not occupy the same state. This gives rise to an effective repulsion between such electrons. The correlation interaction stems from electrons repelling each other due to the Coulomb interaction. To minimize the effects of not knowing E_{xc}^{true}, the Kohn-Sham equation, eq. (3.5), assumes that the ground state density of the original interacting system is equal to that of some chosen non-interacting system that is exactly soluble, with all the difficult parts (the exchange-correlation) included in some approximate functional of the density. Eq. (3.3) is thus rewritten, collecting all the exchange-correlation related terms in an approximative term, $E_{xc}[n]$, in the equation.

$$E[n] = T_0[n(\mathbf{r})] + \int d\mathbf{r} n(\mathbf{r}) V_{ext} + E_H[n(\mathbf{r})] + E_{xc}[n(\mathbf{r})] \tag{3.5}$$

where

$T_0[n(\mathbf{r})]$	Kinetic energy of non-interacting system
$n(\mathbf{r}) = \sum_i^{occ} \lvert\Psi_i(\mathbf{r})\rvert^2$	Electron density
$V_{ext} = -\sum_i^N \frac{Z_I}{\mathbf{r} - \mathbf{R}_I}$	Potential from the nuclei
$E_H[n] = \frac{1}{2} \int \int d\mathbf{r} d\mathbf{r}' \frac{n(\mathbf{r}) n(\mathbf{r}')}{\lvert\mathbf{r} - \mathbf{r}'\rvert}$	Direct Coulomb energy
$E_{xc}[n]$	Exchange and correlation

The basic effect of the KS decomposition is a separation of terms that are in principle possible to calculate from those which are more complicated to determine.

3.2.1 Exchange-correlation approximations

All components in eq. (3.5) might at first glance look similar in composition and complexity. But the truth is that all terms are rather easily solvable but one. The exchange-correlation term, $E_{xc}[n]$, will in all cases, but for the free electron gas, need some approximation to construct a soluble expression.

As the kinetic energy in the Kohn-Sham equation, eq. (3.5), is for a non-interacting system the exchange-correlation term must also include a part of the kinetic energy,

$$E_{xc}[n] = E_{xc}^{true}[n] + (T[n] - T_0[n]) \tag{3.6}$$

There are several approximations available, each suitable for different types of systems and incorporating different types of physics. However, the more sophisticated and accurate functionals are computationally costly. Some of the most commonly used approximations are mentioned below.

Local density approximation

$$E_{xc}[n] = \int d\mathbf{r} n(\mathbf{r}) \varepsilon_{xc}[n(\mathbf{r})] \tag{3.7}$$

The LDA is an approximation which is solely dependent on the local electron density. This can be extended into a Local spin-density approximation, taking the electron spin into account.

Generalized gradient approximation

$$E_{xc}[n] = \int d\mathbf{r} n(\mathbf{r}) \varepsilon_{xc}[n(\mathbf{r})] F_{xc}[n, \nabla n] \tag{3.8}$$

Still a local approximation but improves on the LDA as it also includes the gradient of the density.

Hybrid functionals

$$E_{xc}^{hyb} = \alpha E_x^{HF} + (1 - \alpha) E_x^{DFT} + E_c^{DFT} \tag{3.9}$$

E_x^{HF} is the Hartree-Fock exact exchange functional, while E_x^{DFT} and E_c^{DFT} are the exchange and correlation parts of the density functional. This mixing of exact and approximated exchange energies is proven to have an improving effect on the approximation [6].

3.2.2 Solving the Kohn-Sham equation

Solutions to the Kohn-Sham equation are the one-electron orbitals,

$$\left(-\frac{1}{2}\nabla^2 + v_{ext}(\mathbf{r}) + v_H(\mathbf{r}) + v_{xc}[n(\mathbf{r})] \right) \psi_i(\mathbf{r}) = \epsilon_i \psi_i(\mathbf{r}) \tag{3.10}$$

where v_{ext} is external, v_H the Hartree potential, and v_{xc} the potential connected with the exchange-correlation interaction. To solve this, the orbitals need to be expanded in a basis. There are a few different methods for doing this, one is in a local basis set:

$$\psi_i(\mathbf{r}) = \sum_j C_i j \varphi_j(\mathbf{r}) \tag{3.11}$$

and another is in terms of plane waves:

$$\psi_j(\mathbf{r}) = \frac{1}{\Omega^{1/2}} \sum_j c_g j e^{j\mathbf{g}\cdot\mathbf{r}} \tag{3.12}$$

If a plane wave basis is chosen, one also has to apply pseudopotentials. These potentials replace the core electrons by an effective potential, meaning the calculations can be performed using only the valence electrons.

3.3 Computational implementation

VASP - The Vienna Ab initio Simulation Package

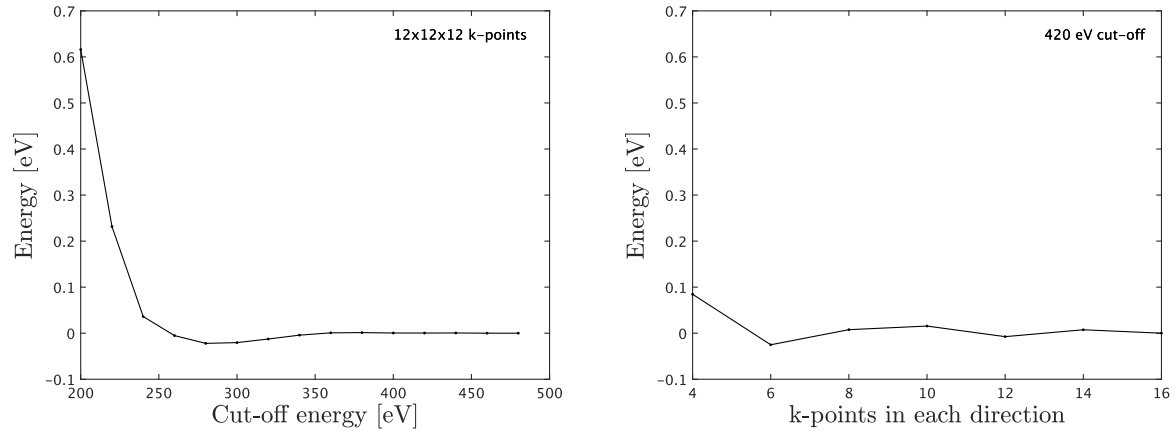
The Density Functional Theory (DFT) was applied with the gradient corrected exchange-correlation functional according to Perdew, Burke, and Ernzerhof (PBE) [7]. In particular, the VASP code was used [8, 9, 10]. The one-electron Kohn-Sham orbitals were expanded in a plane wave basis set with a fixed kinetic energy cut-off. To describe the interaction between the valence electrons and the core, Projected Augmented-Wave (PAW) potentials [11, 12] were used for all elements (palladium, gold, and hydrogen).

ASE - Atomic Simulation Environment

All structures were made using ASE [13], where Vasp was used to calculate the electronic structures. For structural relaxation and bulk moduli calculations, the algorithms provided by ASE was applied.

3.4 Choice of computational parameters

The accuracy of the calculations is determined by a range of computational parameters. Convergence tests are needed in order to determine these parameters. The energy cut-off determines the number of plane waves included in the expansion of the Kohn-Sham orbitals and thus the accuracy of the description of the electronic density. A Monkhorst-Pack grid [14, 15] was used for the integration over the Brillouin zone and the k-point mesh defines how rigorously this is done. Both of these values should be chosen a bit conservatively to allow for some changes in the system structure and composition. The total energy of the Pd and Au systems when sampling over these two variables is presented in Figure 3.1 and based on this, $12 \times 12 \times 12$ k-points and a cut-off energy of 420 eV was chosen for the bulk systems.



(a) *Cut-off energy convergence for Pd.*

(b) *k-point convergence for Pd.*

(c) *Cut-off energy convergence for Au.*

(d) *k-point convergence for Au.*

Figure 3.1: *Convergence of the cut-off energy and number of k-points for the pure Pd and Au bulks.*

For the optimization of the geometry, the structure was considered relaxed when the largest force in the system was smaller than 0.05 eV/Å. The required energetic convergence in the electronic self consistent loop was set to 5 significant digits.

Surface parameters

As the spacing of the k-points is dependent on cell size, larger dimensions requires fewer points and, thus, for the surfaces a $4 \times 4 \times 1$ grid, creating between 6-24 irreducible k-points, was used. In a high symmetry, such as a monometallic surface with the optimal lattice constant, the lower number is employed. When investigating the alloy structures no symmetry is found and the larger number of k-points is necessary. This is in accordance with values used in the literature [16].

Chapter 4

Analyzing first-principles calculations

The result of a DFT calculation is the total energy and the Kohn-Sham orbitals which describe the density. The total energy and the density are fundamental properties which when analyzed gives the desired insight into the system.

4.1 Characterization

When characterizing a material, the first step is to investigate the bulk properties. In this case, using the monometallic systems as a starting point and reference, the structure, composition, and stability of the alloy systems are investigated. The systems are first characterized in bulk with a $1 \times 1 \times 1$ unit cell. Moreover, for the five distinct alloy configurations, the lattice parameter, bulk modulus, and cohesive and mixing energy are determined.

Lattice parameter

The proper lattice parameter is that which gives the lowest energy of the system. Calculating the energy of the system for different values of the lattice constant a and taking the minimum of the least square solution for the third degree fit gives the lattice parameter.

Bulk modulus

The bulk modulus is a measure of the resilience of a solid or liquid to a change in volume, $B = -V\frac{dP}{dV}$, where V is volume and P pressure. Here calculated using the Equation of state function in ASE [17].

Cohesive and mixing energy

The cohesive, or binding, energy in eq. (4.1) is the energy needed to break all the bonds associated to one of the constituent atoms and gives a measure of how stable the compound is.

$$E_{coh} = \frac{E^{bulk} - N \cdot E_{atom}}{N} \tag{4.1}$$

Equation (4.2) gives the mixing energy for the alloy Pd_xAu_y where, in this specific case, $x + y = 4$. The mixing energy gives the tendency for an alloy to mix. The lower the value for E_{mix} the more stable the composite. A positive value indicates that mixing of the materials is thermodynamically unfavorable. A negative value can on the other hand be interpreted as the metals mixing spontaneously, forming a product more stable than its components.

$$E_{mix} = E^{bulk}_{Pd_xAu_y} - \frac{1}{x+y}(xE^{bulk}_{Pd} + yE^{bulk}_{Au}) \tag{4.2}$$

Considering the results of the cohesive and mixing energy, the most energetically favorable and stable alloy composition can be determined.

4.1.1 Surface stability

The energetically preferable (111) surface was modeled with a 2×2 surface cell with six atomic layers. The slabs were separated by 12 Å in the direction normal to the surface. The configurations of interest are the monometallic slabs and those surface configurations possible within the unit cell of the most stable alloy composition. All these alloyed surfaces are redistributions of the atoms in the top four layers of the alloy slab, thus all dimetallic surfaces contain the same number of Au and Pd atoms. To mimic the continuation of the system downwards, the bottom two layers are kept fix and in the bulk configuration throughout all calculations. To evaluate the stability of the surfaces, the surface energy, eq. (4.3), was used.

$$2\sigma = \frac{E_{slab} - N \cdot E_{bulk}}{A} \tag{4.3}$$

Here E_{slab} is the energy of the slab, N the total number of atoms (in this case 24), and E_{bulk} is the energy per atom of the bulk with the same alloy configuration. A is the surface area, which for a 2×2 cell is given by eq. (4.4), where a is the lattice constant.

$$A = \left(\frac{2 * a}{\sqrt{2}}\right)^2 \cdot \sin(60) \tag{4.4}$$

The factor 2 in eq. (4.3) accounts for the fact that there are two surfaces to the slab. For the alloy systems, the two slab surfaces are not always identical. In fact, for most of the structures, the top and bottom surfaces have different configurations, the bottom most layer remaining in the same alloy-confuguration while the top surface changes. To account for this the expression in eq. (4.5) was used instead. Still the value of the lattice parameter, and thus also the value of A, is kept the same for both surfaces of the slab since no surface defects are allowed to form.

$$\sigma + \sigma_{alloy} = \frac{E_{slab} - N \cdot E_{bulk}}{A} \tag{4.5}$$

When solving the surface energy expression, either that in eq. (4.3) or eq. (4.5), a lower value of the energy indicates a more stable configuration.

4.1.2 Adsorption energy

The adsorption energy is a measure of how strongly an adsorbate is bound to the surface. The higher (more negative) the value, the harder it is to remove the adsorbed atom/molecule from the surface. A negative value for the adsorption energy means the adsorbate is energetically more stable in the adsorbed state than as a free molecule. The energy of adsorption was calculated with respect to the hydrogen molecular binding energy in gas phase.

For surface adsorption there are two different kinds of adsorption energies. First the total adsorption energy,

$$E_{ad}^{tot} = E(slab + nH) - E(slab) - \frac{n}{2} \cdot E(H_2) \tag{4.6}$$

where n is the number of adsorbed atoms. Here, all the adsorbed atoms share the total energy added to the system equally, meaning eq. (4.6) gives a measure of the stability of the system. If E_{ad}^{tot} is below zero, the system is stable and if the value decreases with added adsorbates, the system is further stabilized when the coverage increases.

The second adsorption energy is differential.

$$E_{ad}^{diff} = E(slab + nH) - E(slab + (n-1)H) - \frac{1}{2} \cdot E(H_2) \tag{4.7}$$

Using eq. (4.7) yields how the system reacts to addition of one more hydrogen. When at a certain coverage, is the addition of one more atom possible? If the value of E_{ad}^{diff} is negative the last added atom is allowed to adsorb, if positive the last added atom is not stable on the surface.

4.2 Analysis of electronic structure

Having investigated the surface stability and adsorption characteristics, tools are needed for analyzing the results.

4.2.1 Bader analysis

To get a better understanding of what the different configurations actually look like and how they interact on an electron level, a Bader, or charge, analysis can be performed. Bader analysis is a way of using the electron density to distinguish the atoms from each other. This is done by use of 2-D surfaces on which the charge density is a minimum perpendicular to the surface, called zero flux surfaces. Typically these charge minima occur between two atoms which means the charge enclosed within the Bader volume is a good approximation for the charge of the atom. Analyzing how the charge is distributed can show if there, for instance, is charge transfer between the atoms. These calculations are most conveniently performed using the code from the Henkelman group [18].

4.2.2 Local alloy composition

Investigating how the local composition affects the surface systems gives additional insight into why the systems work as they do. Here the relation with surface stability and the impact of adsorption site composition have been investigated. By examining all possible configurations or sites and counting the number of specific nearest (NN) and next nearest neighbours (NNN) the importance and impact of the local composition is determined.

4.2.3 Density of states

Decomposing the electron density, looking at contributions from particular orbitals and from specific atoms, can be very helpful in understanding how characteristics of the system changes. The projections onto the orbital (s, p, and d) can be found using the code provided by the Henkelman group [19]. Once these projections are produced, several interesting properties can be investigated [20]. In all equations below[1], ρ is the sum of the projections onto the wanted orbital; s, p or d.

Total number of states in the band:

$$N_{states} = \int_{-\infty}^{\infty} \rho \mathrm{d}E \tag{4.8}$$

Number of occupied states:

$$N_{occupiedstated} = \int_{-\infty}^{0} \rho \mathrm{d}E \tag{4.9}$$

Average energy of the band (the band center):

$$E_d = \frac{\int \rho \cdot E \mathrm{d}E}{\int \rho \mathrm{d}E} \tag{4.10}$$

Width of the band:

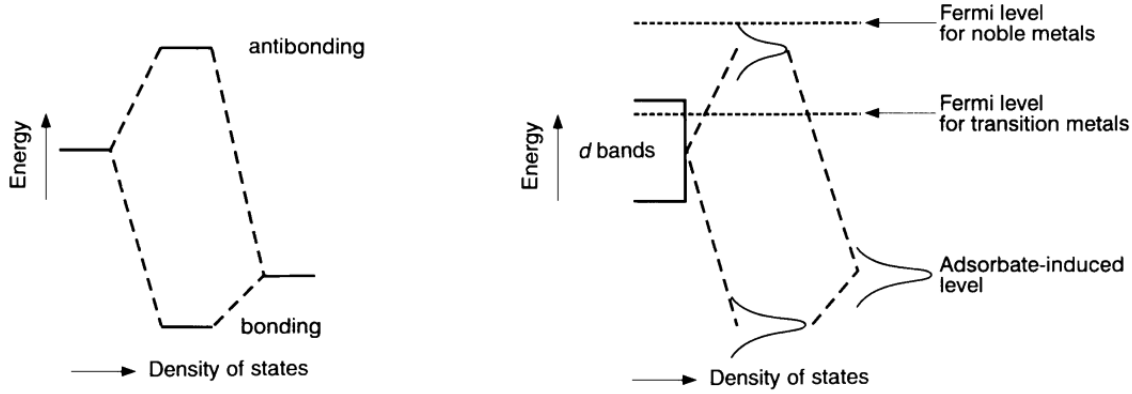
$$W_d^2 = \frac{\int \rho \cdot E^2 \mathrm{d}E}{\int \rho \mathrm{d}E} \tag{4.11}$$

For adsorption processes it is the d-band which is of most interest.

The d-band model

Adding an atom or molecule to the surface of a metal results in a two-level interaction. Firstly, when the two electronic states overlap the Pauli principle dictates the wave functions be orthogonal to each other. This drives up the energy of the system and has a repulsive effect on the adsorbate. However, the overlapping states will also hybridize, forming bonding and antibonding states (Figure 4.1(a)). The bonding state is lower in energy and will be occupied first. If only the bonding state becomes occupied, the hybridization will have an attractive effect, canceling the energy loss caused by the orthogonalization. If both the bonding and antibonding states becomes occupied no energy is gained in the hybridization and the total effect of the interaction is repulsive [21].

[1] Note that the Fermi energy, E_f is set to zero.



(a) *Hybridization of overlapping states.* **(b)** *Interaction between an adsorbate and the metal d-band.*

Figure 4.1: *d-band theory, effects of adsorbate interaction.*

For palladium and gold, the interaction follow this pattern as first the 1s state of the hydrogen interacts with the 4s (Pd) or 6s (Au) to form a deep-lying filled bonding state and an empty antibonding state, making the interaction attractive. Next the bonding state interacts with the d states, or d-bands, of the metals, resulting in an antibonding state just above the metal d-band. If the d-band center of the metal would be lowered, by for instance introduction of a second species in the metal, Figure 4.1(b) illustrates how the energy difference between the d-band and the adsorbate-induced level would decrease, making the bond weaker. For a free atom, the d-band is a single peak at the eigenenergy of the atom.

Results

Chapter 5

Bulk and surface

Investigating the bulk and surface properties is essential if one would like to understand, elaborate on, and find applications for a system. These basic properties affect all aspects and fundamental characteristics of a compound.

5.1 Bulk properties

The results for the bulk phases are collected in Table 5.1. The calculated lattice parameters in Table 5.1a shows a good agreement with literature values [22] while the bulk moduli have a larger discrepancy. For both Pd and Au, the deviation from the experimental value is more than 20 GPa. The underestimation of the bulk moduli have been reported in the literature as well, implying that one reason behind this inconsistency between experiment and calculation is the neglected van de Waals interaction in the PBE functional [23].

From the relative energies in Table 5.1b, the Pd_3Au alloy has the lowest cohesive energy and is, hence, the most stable of the stoichiometries, while the Pd_2Au_2 has the largest tendency for mixing, both in agreement with Ref. [25]. All the alloy stoichiometries have a negative value for E_{mix}. This implies that the hetero-metallic bond are preferable to the homo-metallic bonds and that there is no initial segregation in the alloyed structures. Furthermore, it means that all the alloy stoichiometries are more stable than the monometallic bulks. However, the structure most favorable for mixing does not appear experimentally ([25], [26]) making the second most stable configuration, Pd_3Au, the one which will be used for all further calculations.

Table 5.1: *Bulk properties for Pu, Au, and Pd_xAu_y, where $x + y = 4$. All reference values are from [22] if nothing else is indicated.*

a *Lattice parameter and bulk modulus.*

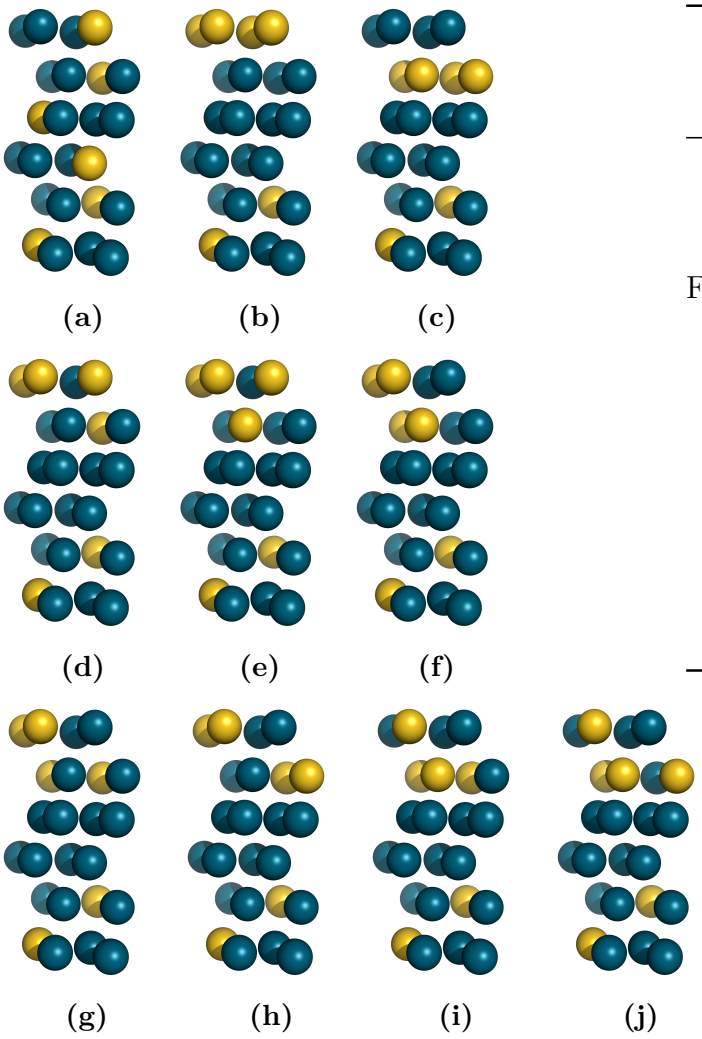
	a [Å]			B [GPa]		
	This work	Exp.	PBE	This work	Exp.	PBE
Au	4.145	4.079	4.180	143	167	131
$PdAu_3$	4.095			150		
Pd_2Au_2	4.046			157		
Pd_3Au	4.000			163		
Pd	3.948	3.881	3.948	169	195	170

b *Cohesive and mixing energy.*

	E_{coh} [eV]		E_{mix} [eV]
	This work	PBE [24]	This work
Au	−3.20	−3.81	0
$PdAu_3$	−3.41		−0.20
Pd_2Au_2	−3.56		−0.33
Pd_3Au	−3.67		−0.29
Pd	−3.76	−3.89	0

5.2 Surface structures and properties

All possible, non-symmetric, configurations of the Pd_3Au alloy surface are presented in Figure 5.1, along with their respective surface energies. Included in the table is also the monometallic slabs of Pd and Au. From this, pure Au is more energetically favorable than pure Pd, and comparing the energies of the alloy surfaces there is an obvious trend of decreasing stability with increasing Pd concentration in the surface layer. Of the studied dimetallic surfaces, the most favorable is that with only Au in the surface layer, and the second most stable are the two slabs with three Au atoms in the top layer. For the bare slab it appears energetically favorable for Au to reside close to the surface.



		Surface energy [meV/Å^2]	
		This work	PBE [22]
	Pd	85	87
	Au	42	37
Figure	(a)	72	
	(b)	67	
	(c)	103	
	(d)	68	
	(e)	68	
	(f)	74	
	(g)	76	
	(h)	78	

Figure 5.1: *All possible, non-symmetric, configurations of the Pd_3Au alloy slab and respective surface energies. The surface layers containing one Au atom are disregarded for the energy calculation. Atomic color code: Palladium (blue) and gold (yellow).*

Charge analysis

For the monometallic slabs, the top and bottom layers have a higher electron density than the atoms inside the slab, which is what would be expected since they have fewer neighbours. When considering the alloy bulk, the Au atoms displays a surplus charge with a mean total charge of 11.08 and, as seen in Table 5.2, all Au atoms located at the surface display the same kind of charge transfer. The surface which was found to be the most stable, that with four Au atoms in the top layer, Figure 5.1(b), would thus have a screening effect towards possible adsorbates and consequently a negative impact on catalytic activity. For top layers composed of both Pd and Au atoms, the result would not be the same. The Pd to Au charge transfer would enable stronger bonds to the Pd atoms and thus facilitate bonding of adsorbates. Introducing Au to the palladium system increases the cohesion of the Pd atoms and also the stability of the system. Thus, a $PdAu_3$ terminated alloy slab would form the most energetically favorable, while still reactive, surface.

Table 5.2: *Charge analysis of bulk and bare surface. The alloy slabs have the mentioned configuration as termination. For the surfaces only the atoms in the surface layer in included.*

		Atom in surface	
		Pd	Au
Bulk	Pd	10	–
	Pd_3Au	9.75	11.075
	Au		11
Surface	Pd	10.03	–
	Pd_3Au	$9.97 - 9.99$	11.17
	$PdAu_3$	9.91	$11.06 - 11.09$
	Au	–	11.02

Local alloy composition

The local alloy composition of the surfaces was investigated to study whether a connection exists between the number of gold neighbours to each Pd atom and the stability of the surface. To do this, the number of Au nearest and next nearest neighbour was counted for each Pd atom in the surface. The result is presented in Figure 5.2, where the number of neighbours are the average for all Pd atoms in the surface layer.

The result in Figure 5.2 shows that the highest stability is found for gold as a nearest neighbour, which is at a distance of approximately 3Å.

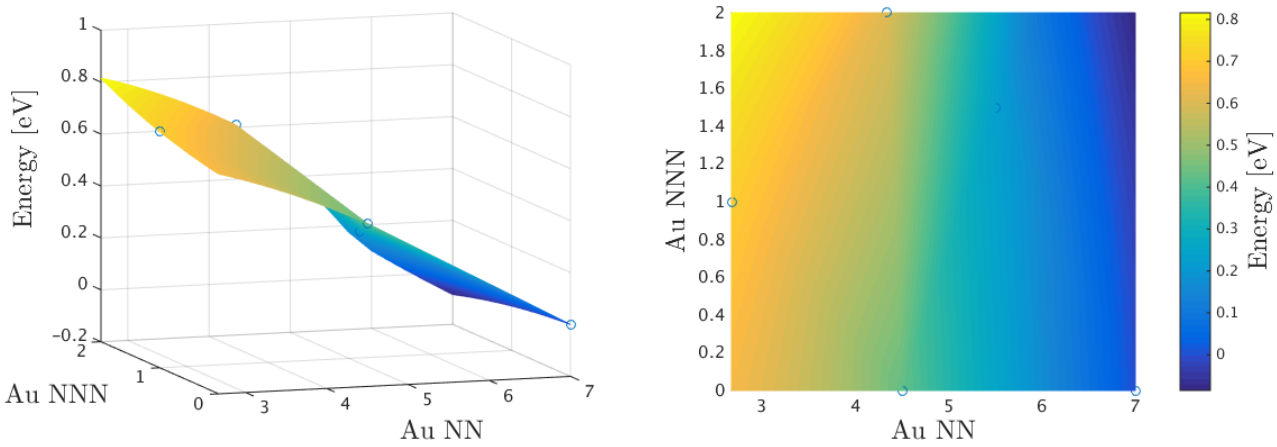


Figure 5.2: *Surface energy as a function of Au nearest (NN) and next nearest (NNN) neighbours. Reference is the lowest known value, all known values are marked by circles. For those surfaces with more than one Pd atom in the top layer, and those instances where the same number of specific neighbours corresponded to different energies, an average has been used. Interpolated.*

5.2.1 Zero-point energy

The above energies does not take the zero-point energy into account. When evaluated for a Pd slab with a hydrogen adsorbate in the fcc hollow the correction was found to be 0.552 eV, while a free hydrogen molecule was calculated to be 0.266 eV.

Chapter 6

Adsorption

When investigating materials for catalytic properties, adsorption is the main feature to study. The reactivity of the surface is what determines if the compound is of interest for further investigation and application. Since there is an interest in knowing the differences between the pure surfaces and the alloy, the monometallic Pd and Au, along with the different terminations of the alloy surface is investigated.

6.1 Surface structures

When introducing a second species to the system, the symmetry of the pure slab is lost. This will affect the number of adsorption sites on the surface. All fcc(111) surfaces have the same four basic surface sites found in Figure 6.1.

6.1.1 Monoatomic surface structures

For the monometallic fcc(111) surface, there are four different kinds of adsorption sites, shown in Figure 6.1. Of these, earlier works have pointed out the fcc and hcp sites as the most energetically favorable [27], a result which is in full agreement with the present results reported in Table 6.1. For the palladium surface, the bridge site was not stable. However, when the x and y-coordinates were constrained to the bridge site and the z-coordinate was relaxed an adsorption energy of -0.48 eV was obtained.

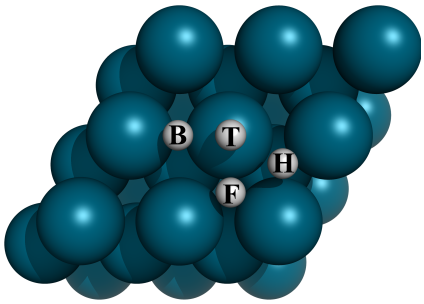


Figure 6.1: *Adsorption sites on a monometallic surface.*

Table 6.1: *Adsorption energies, in eV, for the sites on the monoatomic surfaces. *only allowed to relax in z-direction.*

	Adsorption site			
	fcc	hcp	bridge	ontop
Pd	−0.63	−0.59	−0.48*	−0.11
Au	0.20	0.25	0.27	0.40
Pd, [16]	−0.59	−0.55	−0.44	−0.05
Au, [27]	0.15	0.17	*unstable*	0.33

The positive value of the adsorption energy for all Au sites means that it is not possible for a hydrogen atom to adsorb on the Au surface, a result which might have been hypothesized based on the charge analysis of the bare slab. There is a slight difference between the reference values and the values found in this work; however, the energy difference between the sites are more similar (if excluding the bridge sites on both surfaces).

6.1.2 The alloyed surface structures

When investigating the adsorption, the models for the surfaces are slightly changed. Not only the top layer but also the subsurface, and even deeper lying layers, might impact the adsorption energy. Thus as many layers as possible are kept in alloy configuration, and to keep the number of specific atoms constant in all alloyed surfaces a "compensating" layer is placed just above the two bottom layers, which are frozen, as in Figure 6.2.

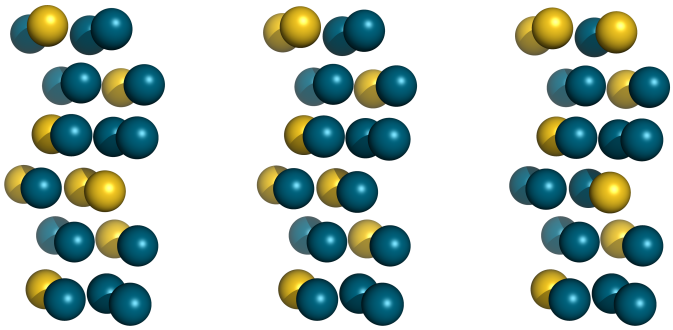


Figure 6.2: *Surface models used in the calculations of adsorption energy.*

Since the adsorption may change the stability of the surface, the most stable version of each of the possible configuration with Pd_xAu_y in the top layer is tested. Calculating the adsorption energy in the ontop position of the Pd atom in the $PdAu_3$ terminated alloy surface, results in $E_{ad} = 0.10$ eV and leads to the assumption that the same kind of sites as on the monometallic palladium will be preferred also on the alloy surface. Thus, only the fcc and hcp sites are studied for adsorption. For these sites there are, in all of these 2×2 unit cell surfaces, a total of six non-symmetrical options, three of fcc and three of hcp type.

¼ Au coverage in the surface layer

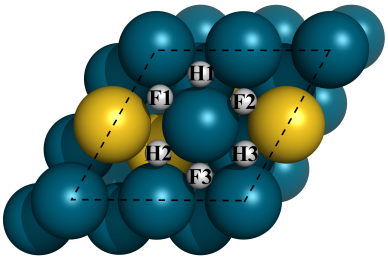


Figure 6.3: *Possible non-symmetric adsorption sites on a Pd_3Au terminated alloy surface.*

Table 6.2: *Fcc and hcp adsorption sites on the Pd_3Au terminated alloy surface. The most stable site is F3 and the second most stable is H1.*

	Adsorption site					
	F1	F2	F3	H1	H2	H3
E_{ad} [eV]	−0.45	−0.43	−0.64	−0.58	−0.39	−0.42

¾ Au coverage in the surface layer

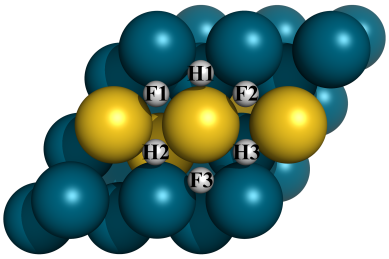


Figure 6.4: *Possible non-symmetric adsorption sites on a Pd_2Au_2 terminated alloy surface.*

Table 6.3: *Fcc and hcp adsorption sites on the Pd_2Au_2 terminated alloy surface. The most stable site is F3 and the second most stable is H1.*

	Adsorption site					
	F1	F2	F3	H1	H2	H3
E_{ad} [eV]	−0.22	−0.16	−0.45	−0.39	−0.17	−0.16

¾ Au coverage in the surface layer

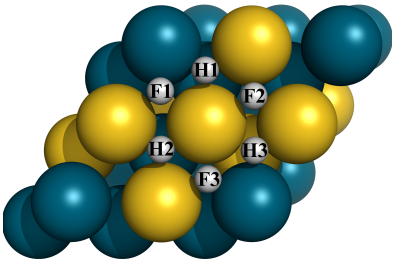


Figure 6.5: *Possible non-symmetric adsorption sites on a $PdAu_3$ terminated alloy surface.*

Table 6.4: *Fcc and hcp adsorption sites on a $PdAu_3$ terminated alloy surface. The most stable site is F3 and the second most stable is H1.*

	Adsorption site					
	F1	F2	F3	H1	H2	H3
E_{ad} [eV]	-0.07	0.17	-0.11	-0.06	0.26	-0.05

For the Pd_3Au surface layer in Figure 6.3, and the Pd_2Au_2 surface layer in Figure 6.4, the hydrogen has the possibility to choose between all the tested sites; however, for the $PdAu_3$ surface layer, Figure 6.5, the sites are loosing their cohesion, and only four of the sites are really possible choices for adsorption. The most stable sites are, for all surface layer configurations, the fcc site with the fewest Au neighbours.

6.2 Bader analysis

When comparing the charge density in the Pd_3Au surface with and without adsorbed hydrogen (as can be found in Table A.3) the charge on the Au atom decreases from 11.17 to 11.16 while that of the palladium drops from 9.97 to 9.92. This is a decrease by 0.05 which is about the same as for the pure Pd surface, decreasing with 0.06/0.04 from 10.03 to 9.97 or 9.99. From Table 6.5, the same surfaces experience a change in charge transfer to the hydrogen atom with changing surface composition. An increasing number of Pd atoms in the surface increases the charge transfer to the adsorbate.

Table 6.5: *Charge analysis of adsorption. The configurations are the first and the last of those in Figure 6.2.The charge is only for the atoms in the top layer, with the values given as an intervall between lowest and highest value.*

		Atom in surface		
		Pd	Au	H
0.25 ML	Pd	9.97 – 9.99	–	1.14
	Pd_3Au	9.92 – 9.94	11.16	1.13
	$PdAu_3$	9.88	11.01 – 11.07	1.07
	Au	–	10.97 – 11.04	1.06

6.3 Local alloy composition

From the results of the adsorption energies and charge analysis there seems to be a clear connection between the number of Au neighbours, the distance to those neighbours, and the adsorption energy of the site. The closer the adsorbed hydrogen is to an Au neighbour, the lower the adsorption energy. Figure 6.6 shows an analysis of the specific neighbours of a single hydrogen atom in the fcc sites of the surfaces in Figure 6.2. For those instances where the same number of specific neighbours corresponded to different energies an average of the adsorption energy has been used.

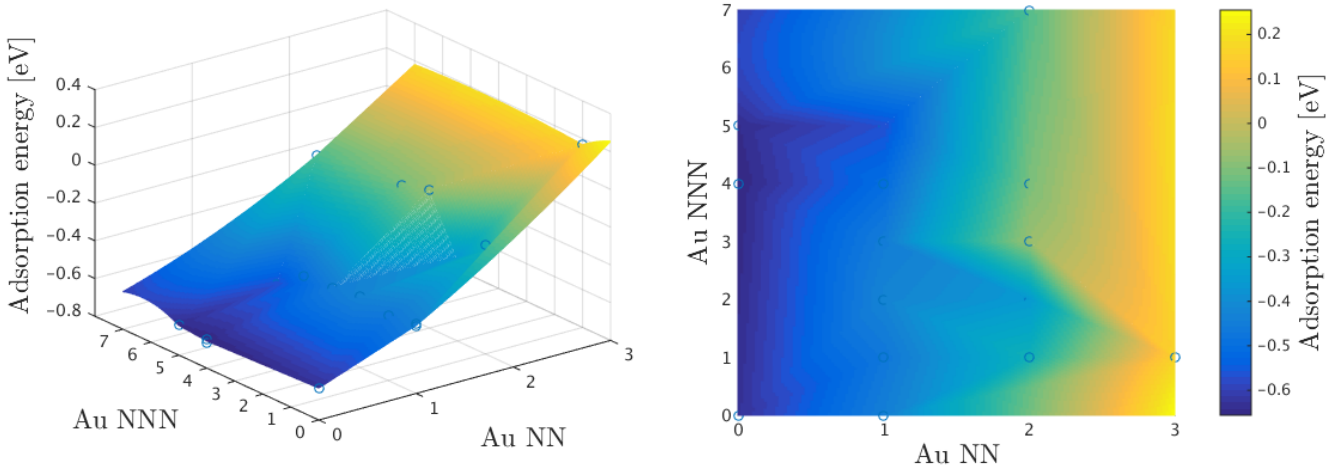


Figure 6.6: *Adsorption energy as a function of Au nearest (NN) and next nearest (NNN) neighbours to the hydrogen. All known values are marked by circles. For those instances where the same number of specific neighours corresponded to different energies an average has been used. Interpolated.*

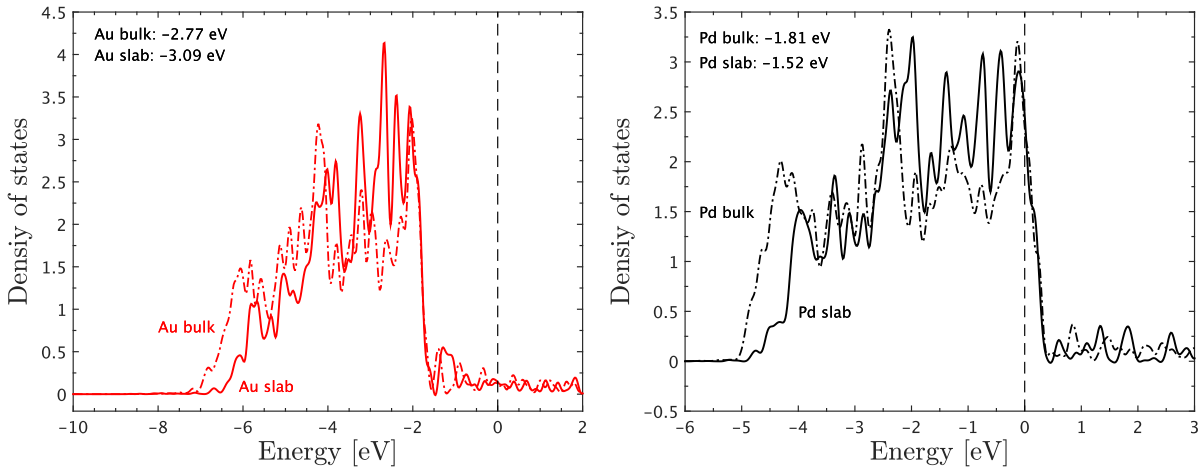
Comparing the results of Figure 6.6 with the analysis of local composition in relation to surface stability, the effect is the opposite. For the adsorption, an increasing number of gold atoms have a negative impact.

6.4 Density of states

The charge and neighbour analysis each add to the explanation of why the adsorption energy of the sites depend on the local alloy composition; however, no clear answer has yet been found. The reasons might lie in how the hydrogen interacts with the surface.

6.4.1 Bulk and surface DOS

For the monometallic compounds the d-band of the bulk and surface systems in Figure 6.7 look as predicted. The more noble Au have a filled d-band and thus, a d-band well below the Fermi energy ($E = E_f = 0$). For Au the d-band is wider than for Pd, implying it is more crowded for the electrons. This is caused by either more neighbours (the d-band for bulk is wider than that for surface) or simply more electrons in the band. For Pd the d-band extends above the Fermi energy since it is not filled.



(a) *Au slab and bulk.* **(b)** *Pd slab and bulk.*

Figure 6.7: *Projected DOS and d-band center for pure Pd, and Au in slab and bulk. Plotted against the Fermi energy.*

In Figures 6.7 to 6.9, the numbers in the upper left corner gives the position of the d-band center for the specified atom. For Figure 6.9 the center value are averages. From Figure 6.8, alloying Pd, with a higher d-band center; and Au, with a lower one, does not give an alloy where all band centers are in the middle of the former values. Rather, the resulting d-band center for the Pd atoms is raised while that for the Au atom is shifted slightly below its former energy. This displacement might be connected with the charge transfer found in the Bader analysis of the systems.

Figure 6.9 shows the d-band for the surfaces in Figure 6.2. For the different surface layer compositions it is the Au d-band which changes the most. In the Pd_3Au terminated slab, the d-band center is at -2.68 eV (Figure 6.9(a)) while for the $PdAu_3$ slab, it has a value of -2.89 eV (Figure 6.9(c)). This 0.21 eV difference is much larger than the 0.01 eV difference in the Pd d-band center, and could be one of the reasons why the local composition of the Pd_3Au surface favors adsorption more than the $PdAu_3$ surface.

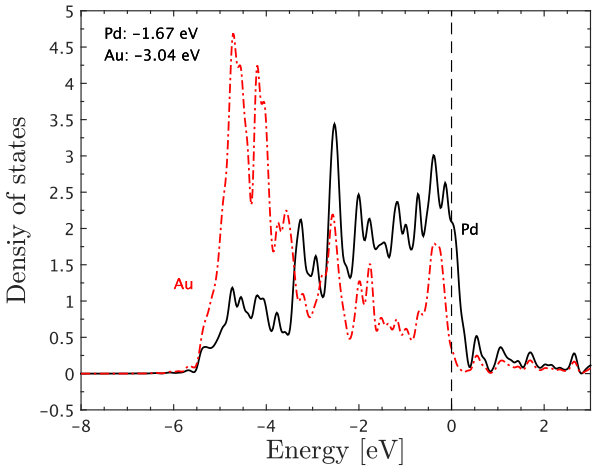
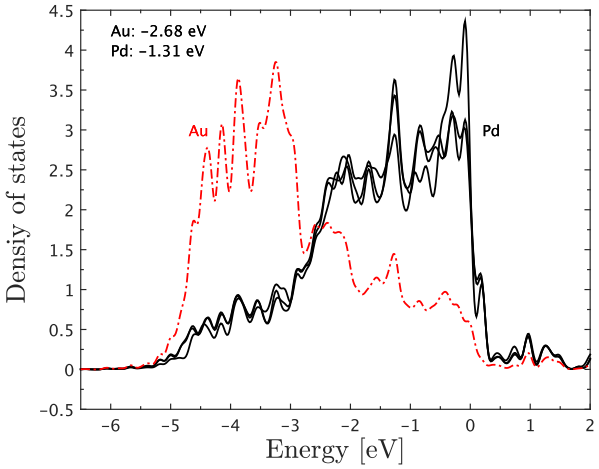
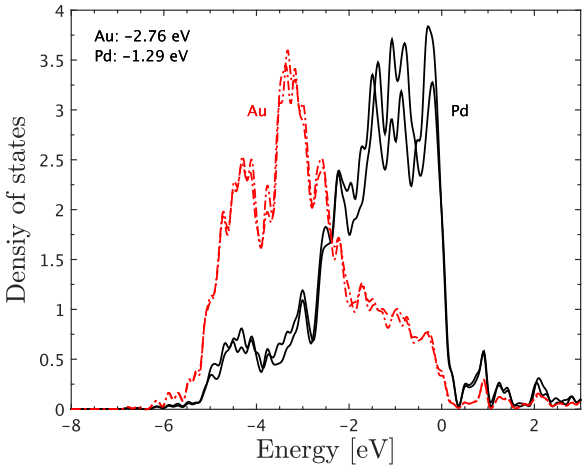


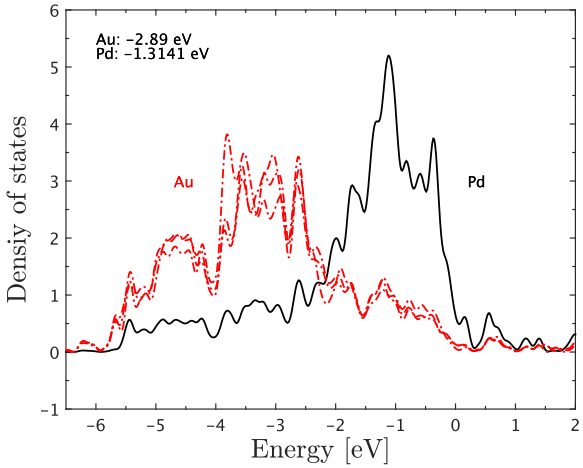
Figure 6.8: *DOS and d-band center for one Pd and one Au atom in the Pd_3Au bulk.*



(a) *Surface layer: Pd_3Au*



(b) *Surface layer: Pd_2Au_2*

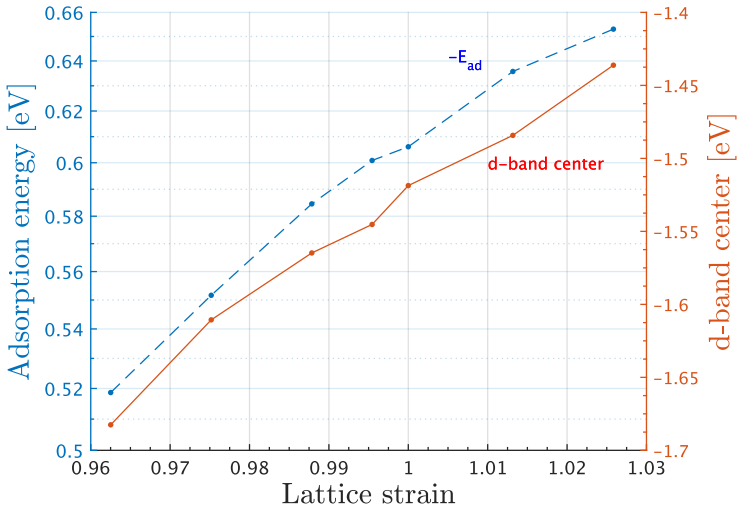


(c) *Surface layer: $PdAu_3$*

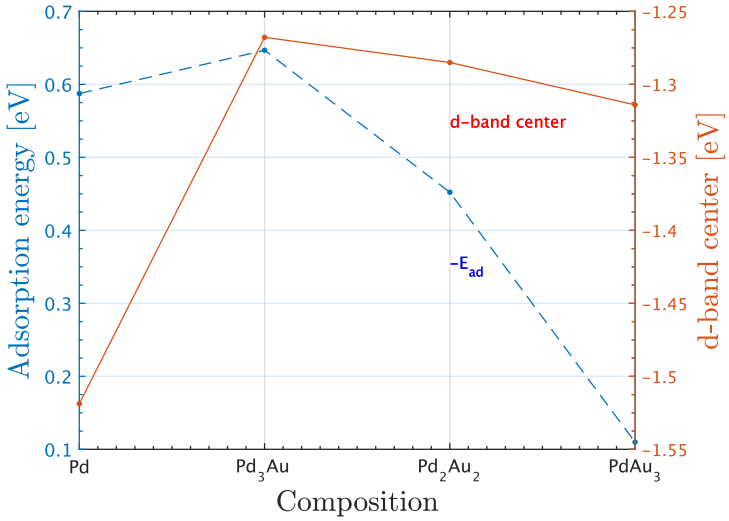
Figure 6.9: *DOS and d-band center for slabs with different alloyed surface compositions. The d-band center averages.*

6.4.2 Lattice strain, d-band center, and adsorption energy

Since the lattice of the alloy is slightly larger than that of the pure palladium the question whether simply a strained lattice has any consequences becomes important. The alloyed surfaces will be affected both by the change in lattice constant induced by the introduction of Au, and by the change in the density of states. The expansion of the lattice will, according to the d-band model and as seen in Figure 6.10(a), raise the d-band center. An effect which should in principle be the same for each of the alloyed surfaces. The change in charge density and DOS on the other hand depends on what neighbours the investigated atom has. Looking at the d-band for the binding palladium atom in the surface, Figure 6.10(b) presents the center energy for the various top layers for 0.25 ML (monolayer[1]), without the hydrogen present.



(a) *Change induced by lattice strain.*



(b) *Change as a result of a changed composition for one Pd atom in the surface. Notice that the relation is inverted, a more negative d-band center gives a less negative adsorption.*

Figure 6.10: *Density of state and adsorption energy*

[1] 1 H atom per 4 metal atoms

6.4.3 The hydrogen DOS

In trying to understand the linear relation between the adsorption energy and the lattice stain in Figure 6.10(a), let's look at the total DOS of two hydrogen atoms, one in an expanded lattice and one in a compressed system, Figure 6.11(a). Integrating the DOS up to the Fermi energy (E=0) gives the total number of electrons in the band. For both hydrogen's in Figure 6.11(a), this integration is approximately one. Thusly, there is no change in the electronic structure of the hydrogen. The bond between the adsorbate and the surface is covantent, as can be understood from the inserted figure in Figure 6.11(b) which shows a magnification of the hybridization between the hydrogen s-states and the metal d-band.
The only clear effect to the electronic structure of the adsorbate is a separation of the bonding (peaks below $E = E_f = 0$)) and the anti-bonding (peaks above $E = E_f = 0$) orbitals. This arises as a compression of the lattice increases the overlap of the states, which is what cause the hybridization. This should have a stabilizing effect on the adsorption, contrary to Figure 6.10(a).

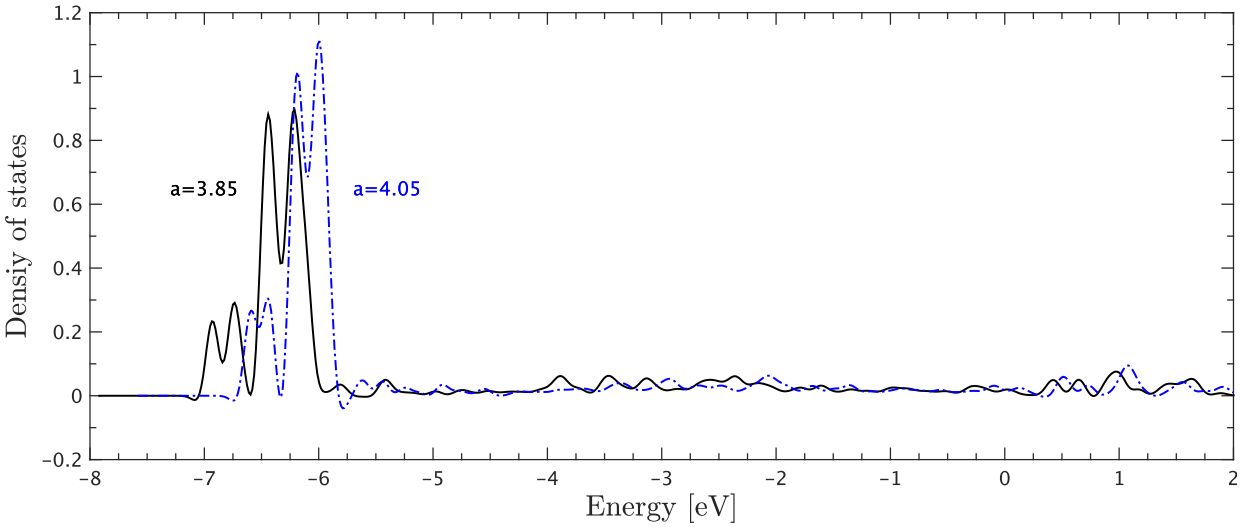
The cohesive energy of the system [28] can be described by a simple Gupta potential [29]:

$$E_c(i) = -\left(\sum_{i\neq j} \xi_0^2 e^{-2q\left(\frac{r_{ij}}{r_0}-1\right)}\right)^{1/2} + \sum_{i\neq j} \epsilon_0 e^{-p\left(\frac{r_{ij}}{r_0}-1\right)} \tag{6.1}$$

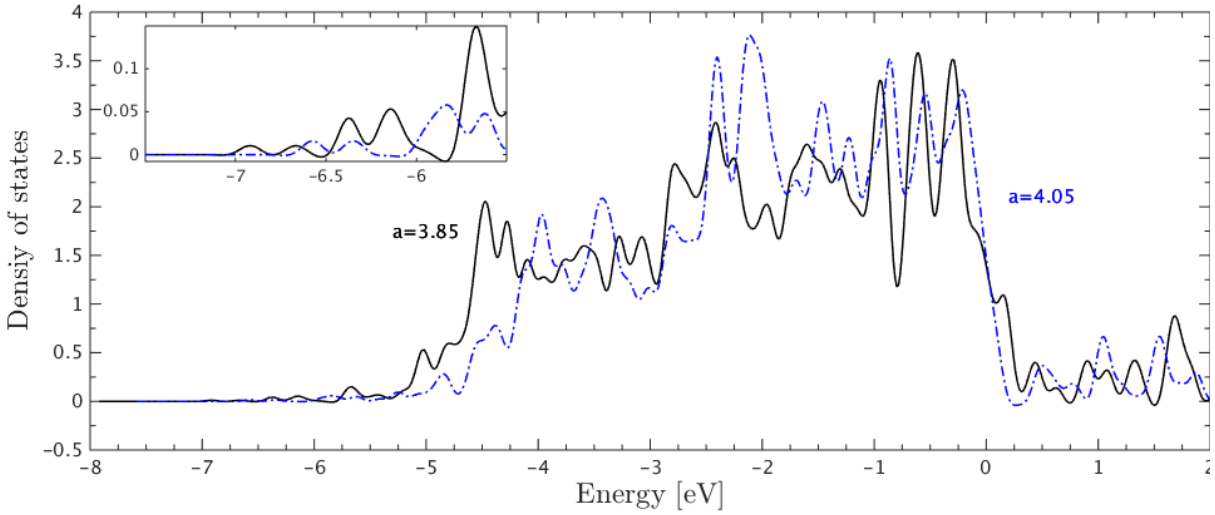
The first term describes the binding, the effect of the orbital overlap, and the second term describes the repulsion in the system. This repulsion is the result of the second effect of adding an adsorbate: repulsion between adsorbate and metal, but also the core-core repulsion between the metal atoms in the surface. In eq. (6.1), the quantities of importance for this discussion is r_{ij}, the distance between the atoms, and r_0, the nearest neighbour distance of the corresponding bulk state. What changes when the lattice in strained is r_{ij}, decreasing for compression and increasing for expansion. A Taylor expansion of the second term

$$\epsilon_0 e^{-p\left(\frac{r_{ij}}{r_0}-1\right)} = \epsilon_0\left(1 - p\left(\frac{r_{ij}}{r_0} - 1\right)\right) + \mathcal{O}$$

reveals a linear dependence of the interatomic distances, just as that seen in Figure 6.10(a). The conclusion is that the repulsive effects of the lattice strain is dominating the interaction, causing a linear decrease in adsorption energy with decreasing lattice parameter. It is also clear that the d-band model is not simply directly applicable in the analysis of the interaction.



(a) *Density of state from one hydrogen on a strained Pd surface.*



(b) *Density of state from one Pd atom in a strained surface.*

Figure 6.11: *Projected total DOS and d-band for adsorbed hydrogen and binding Pd atom. Made using two different lattice parameters, 3.85Å(blue) and 4.05Å(black). (a) Bonding and anti-bonding state of adsorbed hydrogen. (b) d-band of binding Pd atom. Insert of hybridization between Pd d-band and hydrogen states, causing covalent bond at the surface.*

Chapter 7

Effects of hydrogen coverage

Through the performed analysis on surface and adsorption energies it is clear that there are several different sources for the behavior of the systems. The filled d-band of Au, causing occupation of both the bonding and antibonding orbitals, is probably the largest factor behind the weak bonds between the gold atoms and the adsorbate. These weak bonds result in hydrogen preferentially bounding to sites with Pd atoms. Could the stronger bonds between hydrogen and palladium promote diffusion of palladium to the surface layer?

7.1 Surface layer configurations

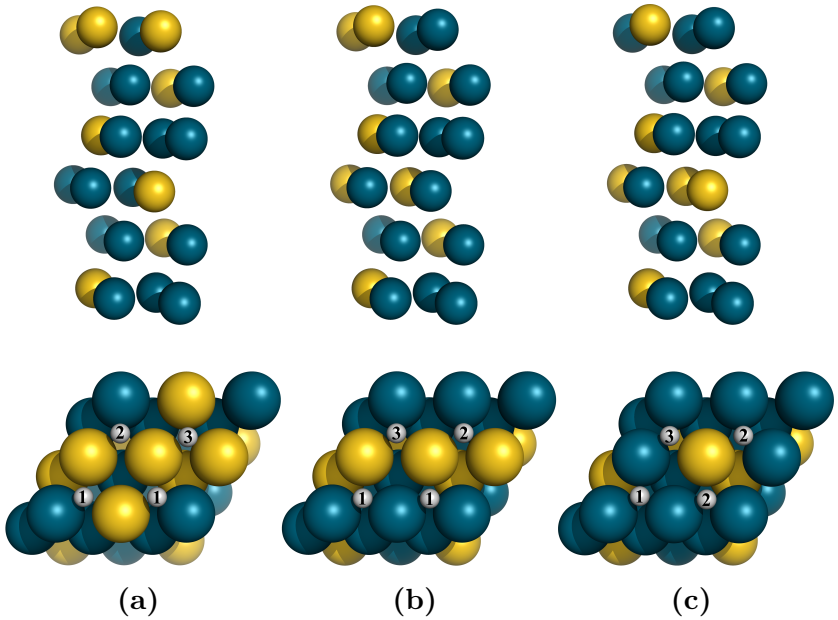


Figure 7.1: *Models of surface layer-configurations for loading. Side and top view. Atomic color code: Hydrogen (white), palladium (blue), and gold (yellow).*

Changing the configuration of the surface layer results in three different slabs, shown in Figure 7.1. The top layers are Pd_xAu_y where $x+y=4$ and $x, y \neq 0$. The three subsequent

layers are kept in bulk configuration, Pd_3Au, while the fourth layer is Pd_yAu_x, to give all surfaces the same total number of specific atoms. The order in which the adsorbates is added is given by the numbers on the hydrogen atoms in the bottom row of Figure 7.1. The sequence is the same for each coverage, starting with the fcc sites with the fewest, and farthest distance to its Au neighbours.

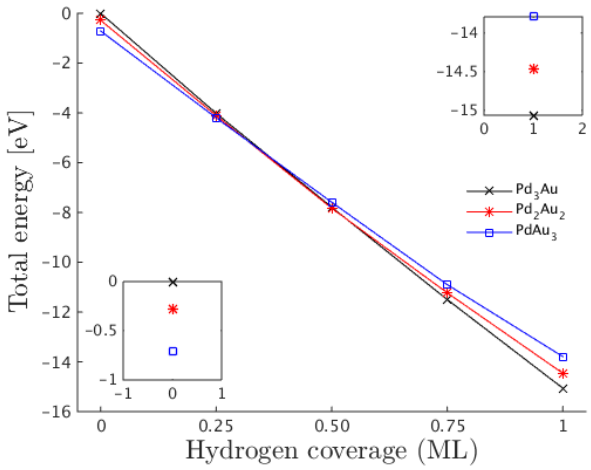


Figure 7.2: *Total energy as a function of coverage for the slabs in Figure 7.1.*

Figure 7.2 shows the total energy of the surfaces using the pure palladium surface as reference. This gives the stability of the systems, and in combination with the adsorption energies it is used to determine the effects of loading. As seen in Figure 7.2, adding hydrogen to the surface changes the preferred surface layer. At 0 ML the surface is already known to be $PdAu_3$, as here confirmed, but for 1 ML this is no longer the case. Instead, it is the Pd_3Au surface which is the preferred one.

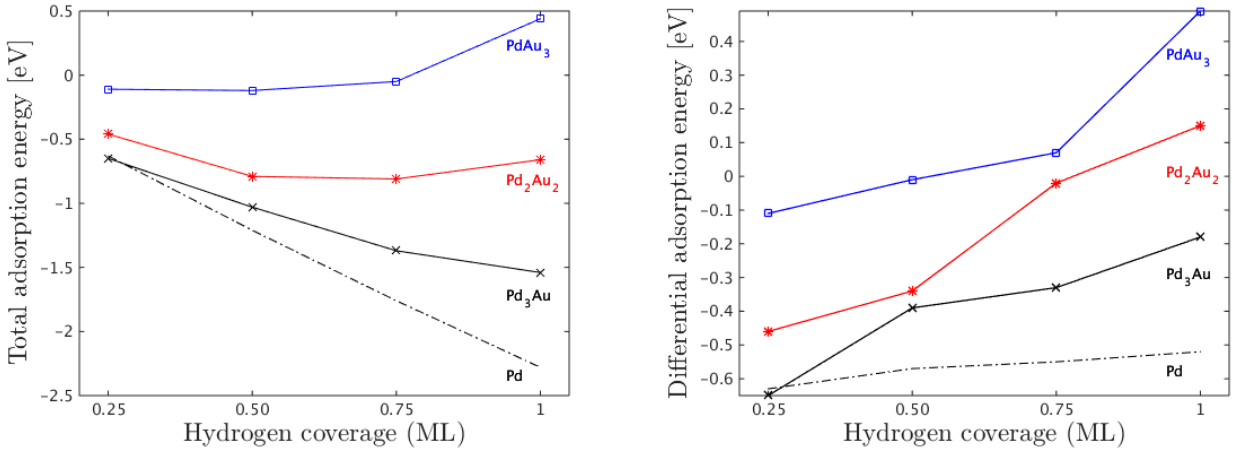


Figure 7.3: *Total and differential adsorption energy as a function of coverage for the surface layer. The studied configuration are those in Figure 7.1. For numerical values see Table A.4.*

In Figure 7.3, the two different adsorption energies show stability of the formed systems and whether the coverage is possible. The calculations show that $PdAu_3$ surface is barely stable for 0 and 0.25 ML and adding a third adsorbate is endothermic. The Pd_2Au_2 surface remains stable for the full coverage; however, adsorbing the last hydrogen is endothermic, meaning 1 ML is never reached. The two surfaces suffering the least deterioration in stability for the highest coverage is the Pd_3Au surfaces along with the Pd reference system. These are the only surfaces which both allow for the full coverage and remains stable.

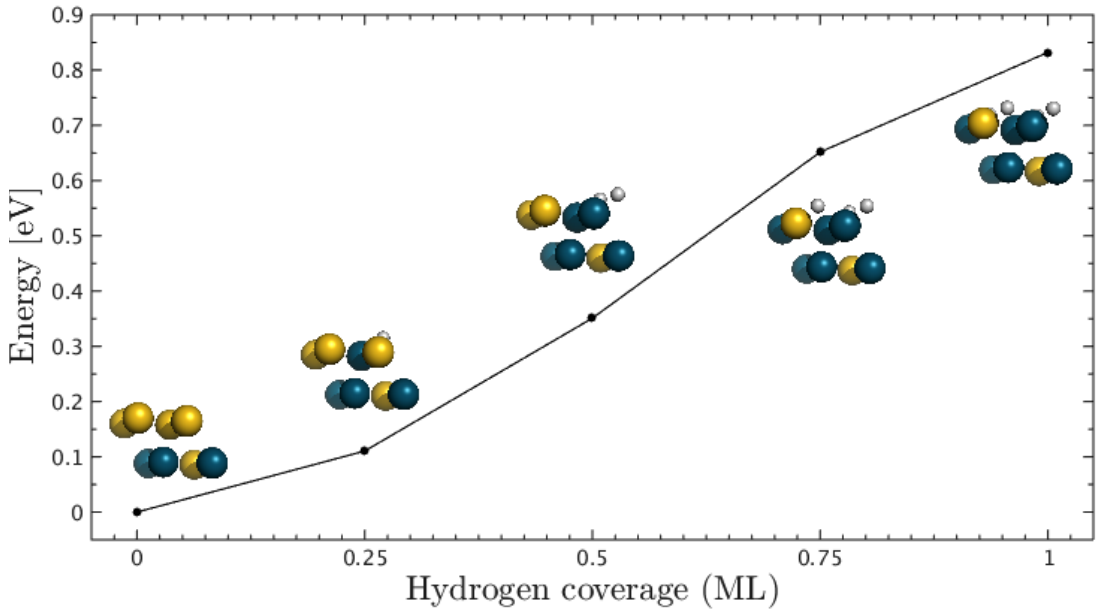


Figure 7.4: *The most energetically stable configuration for each coverage. For the configurations the top two layers of the slabs are shown. The reference is the slab which is the most stable one for 0 ML, corrected for gas phase H_2.*

Thus, when the coverage increases, it is favorable for the Pd contents of the surface layer to increase, as illustrated in Figure 7.4 where the result in summarized.

7.2 Subsurface layer configurations

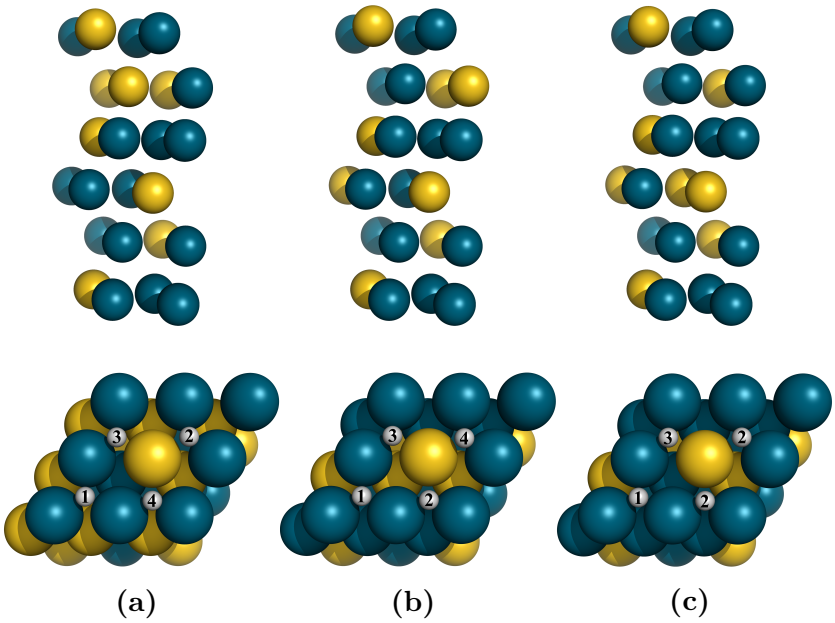


Figure 7.5: *Configuration, and respective top view with sites, of the subsurface layer with the best top layer configuration, Pd_3Au, found in Figure 7.1. All slabs have 8 Au and 16 Pd atoms in total.*

For investigation of the structure of the subsurface layer, the surface layer used is that of the most stable alloy surface at 1 ML, Figure 7.1(c), and the subsurface layers changes configuration according to Figure 7.5.

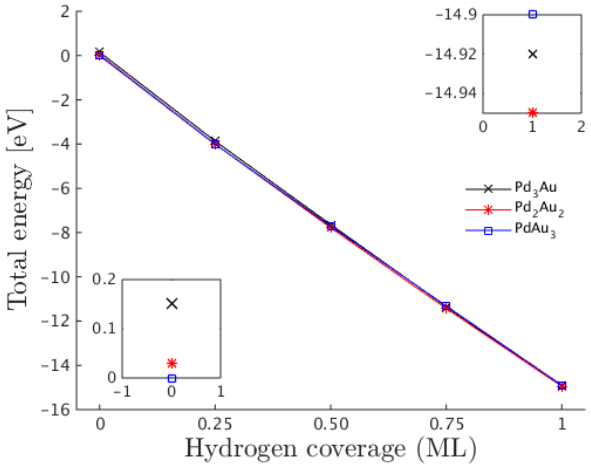


Figure 7.6: *Total energy as a function of loading for the slabs in Figure 7.5.*

From Figure 7.6, the subsurface layers show the same preference towards Pd as the surface layer, although the difference is not as pronounced between the configurations. This smaller variation is due to the subsurface layer having a lesser impact on the adsorption.

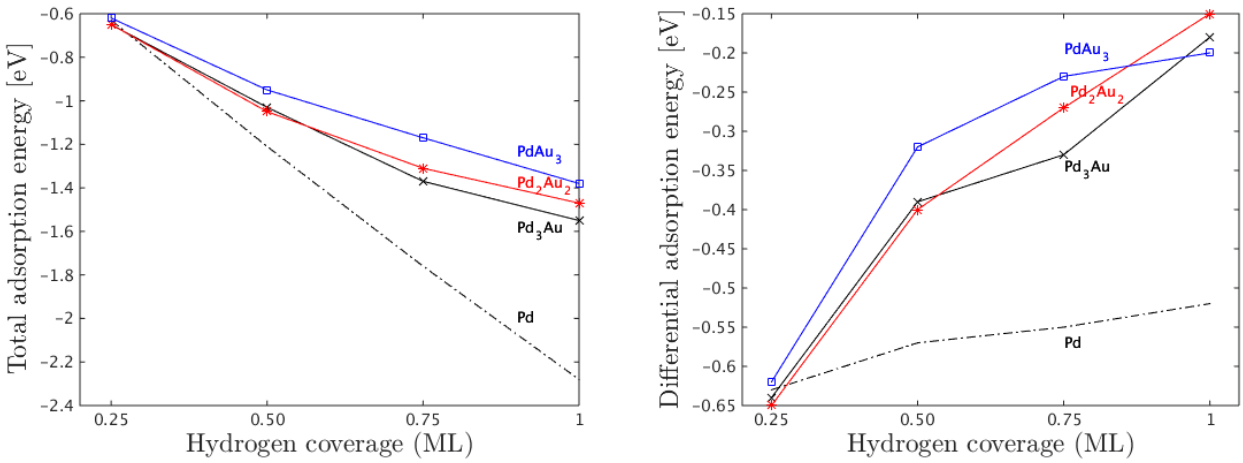


Figure 7.7: *Total and differential adsorption energy as a function of coverage for the subsurface layer. For exact values see Table A.4.*

In Figure 7.8 the result for the subsurface segregation is summarized. For some of the coverages, more than one structure is included. This imply that both are essentially equally stable.

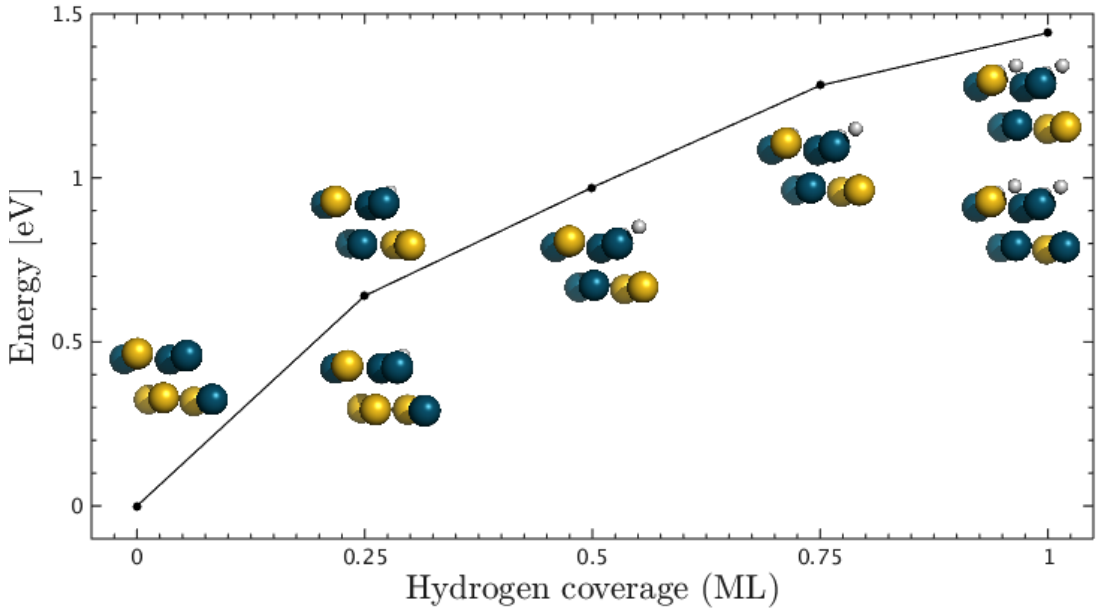


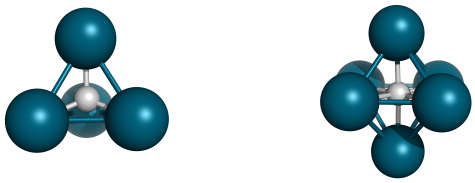
Figure 7.8: *The most energetically stable configuration for each coverage. For the configurations the top two layers of the slabs are shown. The reference is the slab which is the most stable one for 0 ML, corrected for gas phase H_2.*

Chapter 8

Diffusion

A natural extension of adsorption is diffusion. How the adsorbate moves on, through the surface and inside the bulk, will influence what possible applications there are for the material. To study the diffusion, adsorption energies inside the bulk, activation energies, barriers, and energy differences between sites is investigated. The results for pure palladium is presented first. Since the alloy surface has different preferred surface layers depending on coverage, both the one most stable at 0 ML and that at 1 ML has been studied.

An assumption has been made as to which path the hydrogen will diffuse along. Let's assume the adsorbate first is adsorbed in the most stable hcp hollow on the surface, and proceeds to diffuse along the surface to the most stable fcc site. It then enters the slab; through the surface into the O-site and further straight down to the T-site by the third layer. The geometry of these two high symmetry sites in the bulk can be seen in Figure 8.1. The predicted path turns out to be that actually taken in the Pd slab in Figure 8.3(a). To calculate the activation energy for diffusion, the hydrogen is gradually



(a) *T-site* **(b)** *O-site*

Figure 8.1: *High symmetry sites inside the monometallic bulk.*

moved between the sites while only allowed to relax in the directions perpendicular to the path. This method is not the most accurate, for instance using the Nudged elastic band method (NEB) would be more precise, but is chosen considering its considerably lower computational cost. Calculating the energy in each step gives the energy landscape for the diffusion[1], as in Figures 8.2, 8.3(b), 8.6 and 8.7(b). The reference energy used

[1]Note that in the energy profiles, a curve is fitted to the calculated points using MATLAB's spline function to make the energy potentials behavior more visible. This means, the maximums and minimums might not exactly follow the calculation. All conclusion and relation are drawn based on the calculated values, not the fitted curve.

for the landscapes is the energy of the pure bulk, or surface, plus the energy of free atomic hydrogen, E(pure slab/bulk) + $\frac{1}{2}E$(free hydrogen). At each high symmetry site the restrictions on the hydrogen is removed to allow it to properly relax.

8.1 Pd

Bulk

The heat of formation for PdH_1 (with respect to Pd in bulk phase and H_2 in the gas phase), in the O-site, is calculated to be −0.13 eV, slightly below the experimental value of −0.20 eV [30].

	E_{ad} [eV]	
	This work	PBE [31]
T	−0.08	−0.14
O	−0.12	−0.21

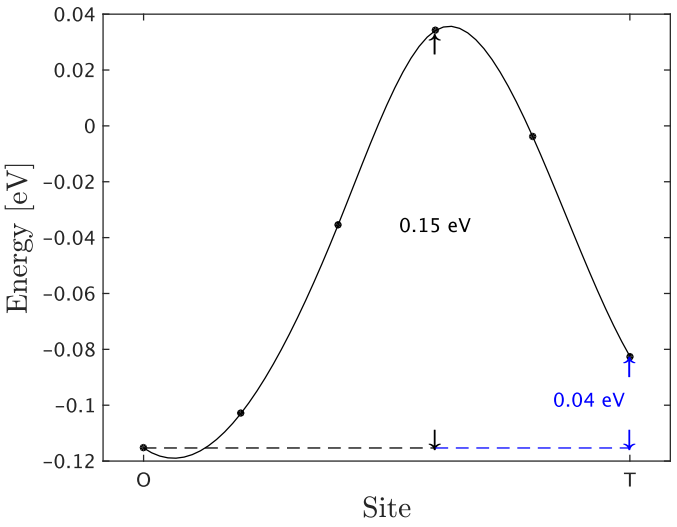
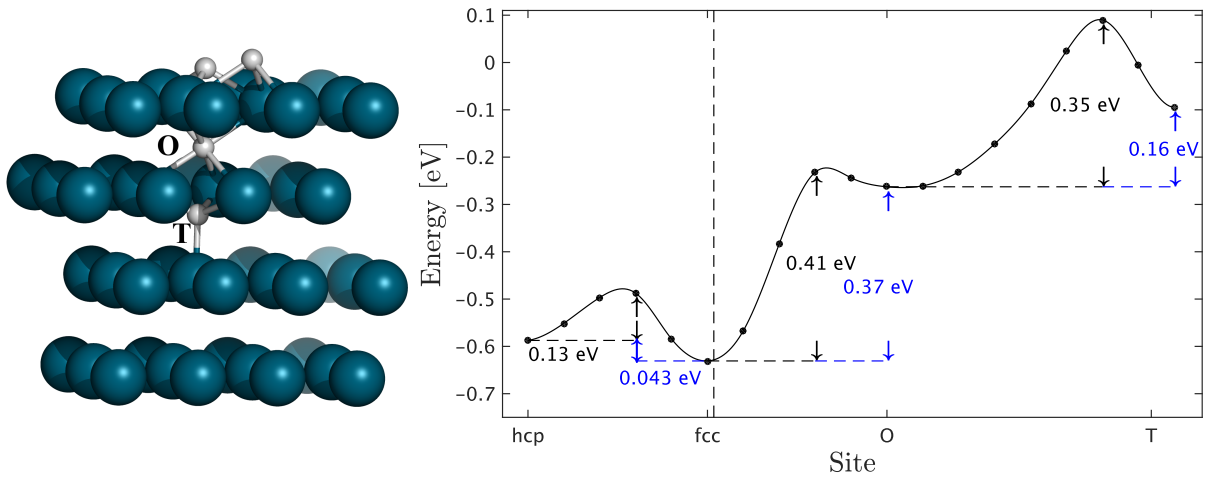


Figure 8.2: *Characteristics of diffusion in the Pd bulk. Adsorption energy and energy profile, with energy differences (blue) and barriers (black).*

The adsorption energies for the two structurally different sites that the hydrogen can occupy in the bulk, one four and one six fold as seen in Figure 8.1, is found in the table in Figure 8.2. Of these the six fold O-site is the most stable, in agreement with [31]. When moving between the sites, the energy landscape is that described by Figure 8.2, having a higher barrier when moving from O to T than from T to O.

Surface

Following the outlined diffusion path, the hydrogen moves straight through the Pd surface as seen in Figure 8.3(a). The energy of the system as the hydrogen passes between the sites is shown in Figure 8.3(b). When the adsorbate has passed the surface layer, marked by a dotted line in Figure 8.3(b), the first site is octahedral. From the energy landscape this is only a semi-stable site where the hydrogen might easily move out instead of farther into the surface. When having passed this site, the tethrahedral site is more stable and the conditions are here comparable to those inside the bulk. The values and general appearance of the energy landscape correspont very well with that found in reference [16], where the fcc to O-site barrier is found at 0.41 eV and the O to T-site at 0.32 eV.



(a) *Diffusion path.*

(b) *Energy profile. The dotted line markes where the adsorbate passes throuch the surface layer.*

Figure 8.3: *Characteristics of diffusion on and through the Pd surface.*

8.1.1 Structural analysis

As for the adsorption, it is of interest to study what effect lattice strain has on the diffusion. When comparing Figures 8.2 and 8.3(b) the energies for the diffusion inside the slab, particularly that of the O-site, does not correlate even though the sites have the same structure. Looking at the interatomic distances in Table 8.1, for the respective sites in the slab and the bulk, gives an explanation as to why.

Table 8.1: *Distances related to the diffusion in Pd. For the slab the interlayer distances are presented with a highest and lowest value to elucidate the structure of the relaxed slab.*

		O-site	T-site	In barrier	$\text{Interlayer}_{\text{max}}$	$\text{Interlayer}_{\text{min}}$
Pd	slab	2.033	1.774	1.684	2.292	2.267
	bulk	1.996	1.783	1.710	2.273	2.273

The spaces in the structures and sites are not the same, and if referencing Tables A.1 and A.2 in the appendix, also plotted here in Figure 8.4, the dependence of the energies on the interatomic distances becomes apparent. For the surface the largest distance, 2.292 Å, is found between the first and second layer. This increases the distances within the site located between the layers, as seen in the O-site values in Table 8.1. As a result the O-site located just below the surface in the slab has a lower energy than the O-site in the bulk, as also evident by the energy landscapes. Just as for the surface adsorption, an expanded lattice has a stabilizing effect. The smallest interlayer distance, 2.267 Å, is found between the second and third layer. When consulting Table 8.1, this does not seem to affect the interatomic distances in the site, but rather the distances between the atoms at the barrier. A shorter distance here increases the activation energy for the diffusion, as can be seen in the top graph in Figure 8.4. Numerical values for the effects of lattice strain is presented in Tables A.1 and A.2.

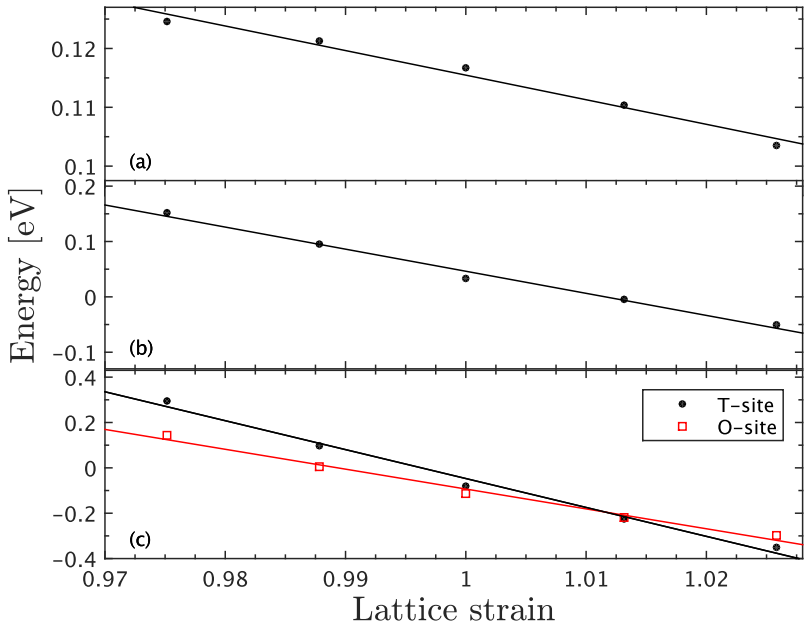


Figure 8.4: *Relation between lattice strain and the energies of the system with* 3.948Å *as the optimal lattice parameter. For all cases the relation is basically linear. a) In the top graph the activation energy for diffusion, from the T to the O-site, is displayed. b) The middle graph shows the energy difference between the two sites. c) The bottom graph displays the adsorption energy of the two sites.*

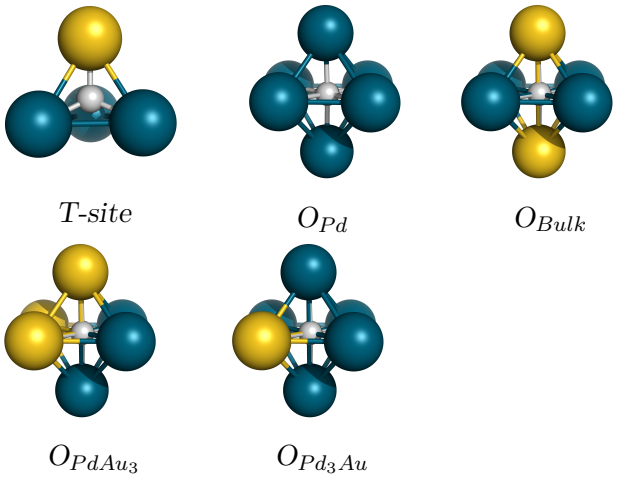
One more interesting effect of straining the lattice is that of graph c) in Figure 8.4. When the expansion of the lattice passes a certain point which of the bulk sites is preferred changes. When the lattice has a strain of 1.0125 the preferred site is not longer the O-site.

8.2 PdAu

As different surfaces where found to be preferred at different coverages, diffusion in both the $PdAu_3$ and the Pd_3Au surfaces has been investigated. Note that, the bulk has the Pd_3Au composition for both surfaces. In the alloy bulk, there are three different high symmetry sites, presented in the top row of Figure 8.5. The two sites in the bottom row of Figure 8.5 are the sites the hydrogen reaches when passing through the fcc hollow in the surface layer. Since the surface composition of the slabs are different, the geometry of this first site also differs.

Bulk

The heat of formation for Pd_3AuH_1 (with respect to Pd_3Au in bulk phase and H_2 in the gas phase), for H in the most stable O-site, is calculated to be -0.19 eV. The energy landscape for the diffusion inside the Pd_3Au bulk, Figure 8.6, indicates that the T-site in Figure 8.5 in not stable. When reaching this site the hydrogen directly diffuses into the adjacent O_{Pd}-site. The only energetically preferred site is that consisting exclusively of Pd atoms.



	E_{ad} [eV]
T	–
O_{Pd}	−0.19
O_{Bulk}	0.13
O_{PdAu_3}	0.19
O_{Pd_3Au}	0.15

Figure 8.5: *High symmetry sites in the alloy bulk and in the two different surfaces. O_{PdAu_3}, and O_{Pd_3Au}, only exists in the $PdAu_3$, and Pd_3Au, terminated alloy surface, respectively. Here presented with their respective adsorption energy.*

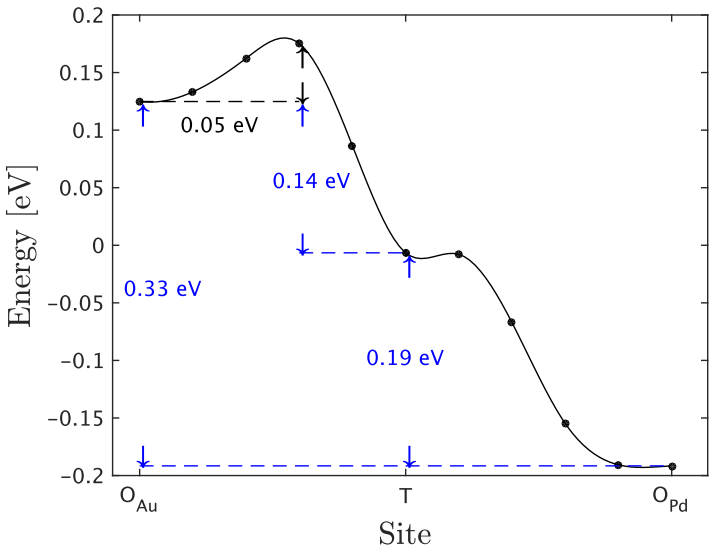
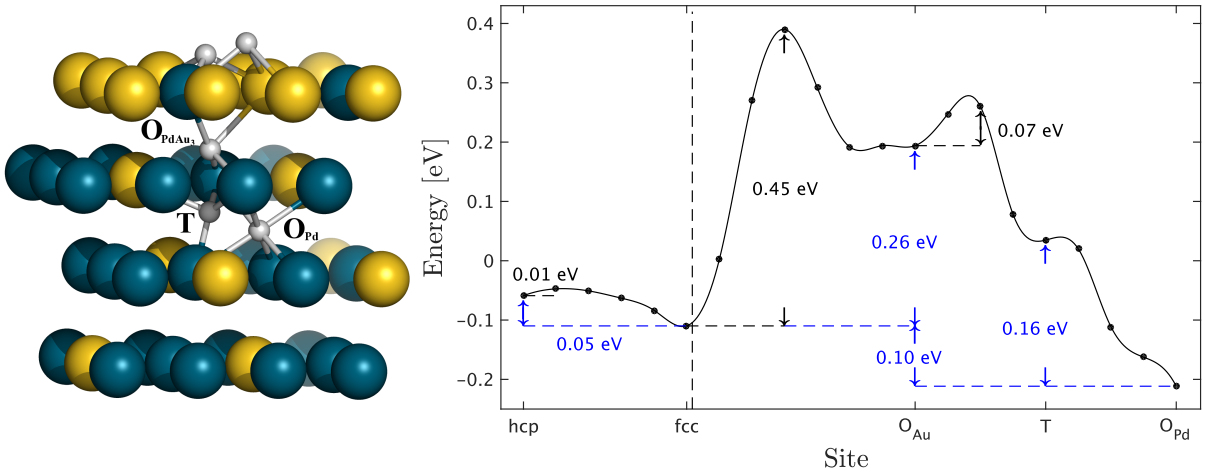


Figure 8.6: *Characteristics of diffusion in the Pd_3Au bulk.*

8.2.1 Bare $PdAu_3$ terminated alloy surface

When the hydrogen passes through the fcc hollow on the surface, the first site it encounters is the O_{PdAu_3}-site in Figure 8.5. Relaxed in this site, the distances inside the site is to large for the hydrogen to connect to all the atoms. As the preference is towards Pd, all Pd atoms are reached but only one of the three Au atoms. Just as for the bulk the T-site between layer two and three is not stable, the hydrogen continues past it and deeper into the slab. Comparing the landscape in Figures 8.6 and 8.7(b), the diffusion between the T and O-sites has only a slight variation, leading to the conclusion that by the third layer, the slab has the same properties as the bulk.



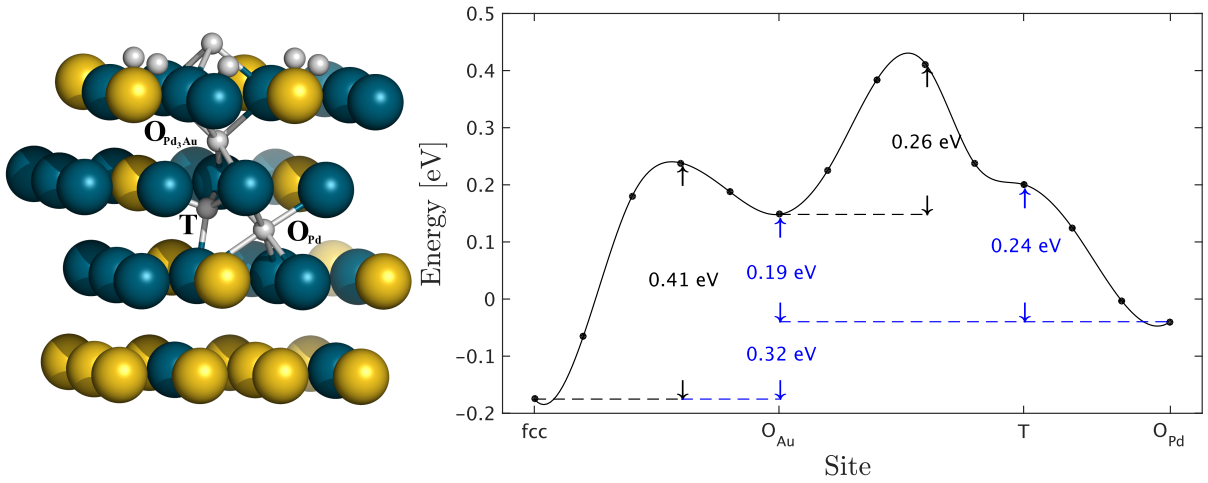
(a) *Diffusion path.*

(b) *Energy profile. The dotted line markes where the adsorbate passes throuch the surface layer.*

Figure 8.7: *Characteristics of diffusion through the $PdAu_3$ terminated alloy surface.*

8.2.2 Loaded Pd_3Au terminated alloy surface

As a higher coverage prefers a high fraction of Pd in the top layer, the diffusion in the Pd_3Au surface is performed with full coverage. For this surface, no on-surface diffusion has been allowed. The hydrogen directly enters the slab through the most stable fcc hollow. The first site it encounters is the O_{Pd_3Au}-site in Figure 8.5. When relaxed in this site, the preference towards Pd causes the adsorbate to only form bonds with the Pd atoms. Consistent with the earlier results, the hydrogen passes straight through the T-site between the second and third layer, landing in the preferred O_{Pd}-site. Comparing the energy of the O_{Pd}-site in the surface and the bulk, bulk conditions are not reached at this depth of the surface.



(a) *Diffusion path.* **(b)** *Energy profile.*

Figure 8.8: *Characteristics of diffusion through the loaded Pd_3Au terminated alloy surface.*

8.2.3 Structural analysis

Only considering the diffusion from the fcc surface hollow, down to the O_{Pd}-site by the third layer, there are a few significant differences for the profiles of the two surfaces. The first barrier is approximately the same, only differing by 0.04 eV. The first subsurface sites have different geometry for the different surfaces, both in composition and in interatomic distances (found in Table 8.2). For the $PdAu_3$ surface, the average distance between the adsorbate and the atoms of the metal is 2.088 Å, being the most spacious of all subsurface sites. However, from the adsorption energies in Figure 8.5, it is also the least preferred O-site. The O_{PdAu_3}-site is composed of three Au and three Pd atom, this makes it the site with the highest Au concentration. Comparing with the O_{Pd_3Au}-site, with interatomic distances of 2.043 Å, one Au and five Pd atoms, and 0.15 eV in adsorption energy, shows that the increasing number of Au atoms has a dominating effect over that of the increased distances.

Table 8.2: *Distances related to the diffusion in PdAu. The values are averages. For the surfaces, the barrier is that between the first subsurface O-site and the subsequent T-site.*

	O_{Pd}-site	T-site	O_{Au}-site	Barrier O -> T	Layer
Alloy bulk	2.016	–	2.020	1.756	2.304
$PdAu_3$ surface	2.020	–	2.088	1.709	2.323
Pd_3Au surface	2.020	–	2.043	1.716	2.351

The next barrier is that between the O-site and the T-site closest to the surface. In the Pd_3Au slab the barrier is 0.19 eV higher than in the $PdAu_3$ slab. This despite the larger distances in the barrier, and likely due to the difference in Au distribution. This high second barrier in the Pd_3Au surface results in a total barrier of 0.58 eV to reach the third layer of the slab. At this third layer the bulk conditions are not yet reached for the loaded slab. As the interatomic distances in the O_{Pd}-sites are the same in both slabs this might be due to the Au rich fourth layer of the Pd_3Au terminated slab.

Epilogue

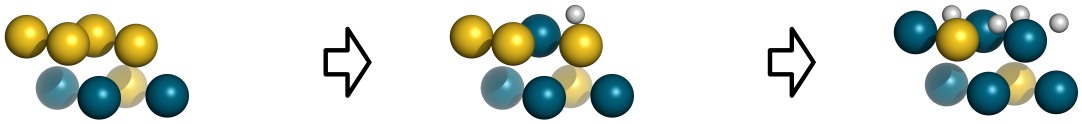
Chapter 9

Conclusion

This thesis sought to characterize the bulk and the fcc(111) surface of the PdAu alloy. For the bulk composition, the second most stable composition, Pd_3Au, was chosen. This due to the lack of experimental results for the most stable Pd_2Au_2 composition. The composition of the alloy surface turned out to depend on the hydrogen coverage. Investigating the diffusion barriers through the surfaces and inside the bulk, showed how alloying palladium with gold changes the energy landscape.

9.1 Segregation of surface metal atoms

Increasing the coverage increasingly promotes palladium segregation to the surface.



For the most stable bare surface, the second layer contains only one Au atom. In this study, this subsurface layer cannot be filled with gold, since the model used contained a total of just six Au atoms. However, from the stability dependence of the nearest and next nearest neighbours in Figure 5.2, a reasonable assumption would be that a surface and subsurface layer composed solely of Au atoms would be even more preferable than the surface found here. The same reasoning implies that the most preferred surface composition for the full coverage would be that of the two surface layers entirely consisting of palladium atoms.

9.2 Diffusion of hydrogen

From the energy landscapes of Figures 8.2, 8.3(b), 8.6 and 8.7(b), the properties of the alloyed surface differs from those of the pure palladium. To illustrate this, the two energy landscapes are plotted together in Figure 9.1. Alloying with Au decreases the barrier to enter the surface; however, once inside the barrier for diffusion in the bulk is increased.

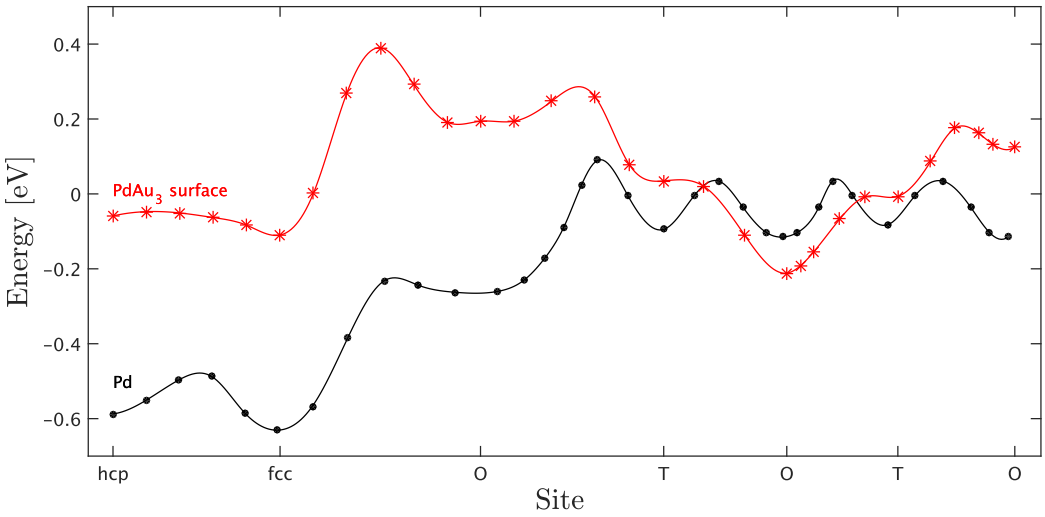


Figure 9.1: *Energy landscapes of Pd and $PdAu_3$ terminated alloy surface.*

Chapter 10

Outlook

To fully characterize the behavior of the PdAu system there are a few appropriate next steps. Investigation of the beta phase is one. In particular studying hydride formation for the alloy and how this phase affects adsorption. Also considering diffusion of the metal atoms is important. Is the implied segregation of the surface atoms realizable, or is the barrier for metal diffusion too large? It might also be interesting to further investigate the surface structure of the alloy. Not only looking at the composition, but also the structure of the surface. Might there be surface segregation with formation of "islands" of gold or palladium? For further application within the area of catalysis, the same investigation of segregation and diffusion could be done for the PdAu nano particles.

Bibliography

[1] D.G. Lovering and Ross A. Lemons. Proceedings of the grove anniversary fuel cell symposium fuel cells for transportation. *Journal of Power Sources*, 29(1):251 – 264, 1990.

[2] Laiyuan Chen, Bong-Kyu Chang, Yong Lu, Weiguo Yang, and Bruce J. Tatarchuk. Selective catalytic oxidation of co for fuel cell application. Fuel Chemistry Division Preprints, 47(2), 609, 2002.

[3] Chandrashekhar G. Sonwane, Jennifer Wilcox, and Yi Hua Ma. Solubility of hydrogen in pdag and pdau binary alloys using density functional theory. *The Journal of Physical Chemistry B*, 110(48):24549–24558, 2006. PMID: 17134214.

[4] J.C. Amphlett, R.M. Baumert, R.F. Mann, B.A. Peppley, P.R. Roberge, and A. Rodrigues. Inhomogeneous electron gas. *Phys. Rev.*, 136:B864–B871, Nov 1964.

[5] Ander Hellman. Density functional theory. Lecture notes in Computational Material Physics, Chalmers University of Technology, 2016.

[6] John P. Perdew, Matthias Ernzerhof, and Kieron Burke. Rationale for mixing exact exchange with density functional approximations. *The Journal of Chemical Physics*, 105(22):9982–9985, 1996.

[7] John P. Perdew, Kieron Burke, and Matthias Ernzerhof. Generalized gradient approximation made simple. *Phys. Rev. Lett.*, 77:3865–3868, Oct 1996.

[8] G. Kresse and J. Hafner. *Ab initio* molecular dynamics for liquid metals. *Phys. Rev. B*, 47:558–561, Jan 1993.

[9] G. Kresse and J. Hafner. *Ab initio* molecular-dynamics simulation of the liquid-metal–amorphous-semiconductor transition in germanium. *Phys. Rev. B*, 49:14251–14269, May 1994.

[10] G. Kresse and J. Furthmüller. Efficiency of ab-initio total energy calculations for metals and semiconductors using a plane-wave basis set. *Computational Materials Science*, 6(1):15 – 50, 1996.

[11] P. E. Blöchl. Projector augmented-wave method. *Phys. Rev. B*, 50:17953–17979, Dec 1994.

[12] G. Kresse and D. Joubert. From ultrasoft pseudopotentials to the projector augmented-wave method. *Phys. Rev. B*, 59:1758–1775, Jan 1999.

[13] S. R. Bahn and K. W. Jacobsen. An object-oriented scripting interface to a legacy electronic structure code. *Comput. Sci. Eng.*, 4(3):56–66, MAY-JUN 2002.

[14] Hendrik J. Monkhorst and James D. Pack. Special points for brillouin-zone integrations. *Phys. Rev. B*, 13:5188–5192, Jun 1976.

[15] James D. Pack and Hendrik J. Monkhorst. "special points for brillouin-zone integrations"—a reply. *Phys. Rev. B*, 16:1748–1749, Aug 1977.

[16] Sampyo Hong and Talat S. Rahman. Adsorption and diffusion of hydrogen on pd(211) and pd(111): Results from first-principles electronic structure calculations. *Phys. Rev. B*, 75:155405, Apr 2007.

[17] Equation of state. Available at `https://wiki.fysik.dtu.dk/ase/tutorials/eos/eos.html`(2015/11/16).

[18] Code: Bader charge analysis. Available at `http://theory.cm.utexas.edu/henkelman/code/bader/` (2016/01/02).

[19] Vtst-tools. Available at `http://theory.cm.utexas.edu/vtsttools/scripts.html` (2016/02/04).

[20] March 8, 2016. Available at `http://gilgamesh.cheme.cmu.edu/doc/software/jacapo/2-bulk/2.3-atom-projected-dos/2.3.0-atom-projected-dos.html` (2016/03/08).

[21] B. Hammer and J. K. Norskov. Why gold is the noblest of all the metals. *Nature*, 376(6537):238–240, 1995.

[22] Fabien Tran, Robert Laskowski, Peter Blaha, and Karlheinz Schwarz. Performance on molecules, surfaces, and solids of the wu-cohen gga exchange-correlation energy functional. *Phys. Rev. B*, 75:115131, Mar 2007.

[23] Julia Alwan. Study of van de waals effects in gold-thiolate systems. Master's thesis, Chalmers university of technology, 2015.

[24] Faye Pittaway, Lauro Oliver Paz-Borbón, Roy L. Johnston, Haydar Arslan, Riccardo Ferrando, Christine Mottet, Giovanni Barcaro, and Alessandro Fortunelli. Theoretical studies of palladiumgold nanoclusters: Pdau clusters with up to 50 atoms. *The Journal of Physical Chemistry C*, 113(21):9141–9152, 2009.

[25] Rémi Marchal, Alexander Genest, Sven Krüger, and Notker Rösch. Structure of pd/au alloy nanoparticles from a density functional theory-based embedded-atom potential. *The Journal of Physical Chemistry C*, 117(42):21810–21822, 2013.

[26] Giuseppe Zanti and Daniel Peeters. Dft study of bimetallic palladiumgold clusters pdnaum of low nuclearities. *The Journal of Physical Chemistry A*, 114(38):10345–10356, 2010. PMID: 20812747.

[27] Viktor Nilsson. Adsorbate induced core level shifts of transition metal surfaces. Master's thesis, Chalmers university of technology, 2013.

[28] Henrik Grönbeck. *On the structure of and bonding in metal clusters.* PhD thesis, Chalmers university of technology, 1996.

[29] Raju P. Gupta. Lattice relaxation at a metal surface. *Phys. Rev. B*, 23:6265–6270, Jun 1981.

[30] Georg Alefeld and Johann Völkl. *Hydrogen in Metals II.* Springer Berlin Heidelberg, 1978.

[31] Henrik Grönbeck and Vladimir P. Zhdanov. Effect of lattice strain on hydrogen diffusion in pd: A density functional theory study. *Phys. Rev. B*, 84:052301, Aug 2011.

Appendix A

Numerical values

Properties of the materials

Effects of lattice strain

Table A.1: *Energy dependence of lattice compression. 3.948* Å *is the optimal lattice parameter.* E_{bulk} *= energy of the bulk,* ΔE *= energy difference between O and T-site.*

	E_{bulk}	ΔE	E_{ad} [eV]		Barrier [eV]	
a			T	O	T → O	O → T
4.050	−165.307	0.051	−0.351	−0.299	0.103	0.053
4.000	−166.379	0.005	−0.223	−0.219	0.110	0.106
3.948	−166.844	0.033	−0.082	−0.115	0.117	0.149
3.930	−166.836	0.064	−0.008	−0.071	0.118	0.182
3.900	−166.587	0.095	0.098	0.004	0.121	0.216
3.850	−165.468	0.152	0.297	0.145	0.125	0.277
Reference						
3.930		0.07				0.22

Table A.2: *Interatomic distances for Pd with strained lattice. The optimal lattice parameter is 3.948* Å*. The values are averages.*

	Distance [Å]		
a =	O-site	T-site	Layer
4.050	2.043	1.819	2.362
4.000	2.019	1.799	2.315
3.948	1.996	1.783	2.273
3.930	1.988	1.771	2.263
3.900	1.975	1.759	2.245
3.850	1.952	1.738	2.210
Reference			
3.930		1.98	

Charge analysis

Table A.3: *Charge analysis. Only including the atoms in the top layer with the given configurations. For 0 ML the configurations are those in Figure 5.1, for 0.25 ML those in Figure 7.1 are used. Bulks are 2x2x2 unit cell.*

		Surface atom		
		Pd	Au	H
Bulks	Pd	$9.944 - 10.075$	-	-
	Pd_3Au	$9.927 - 10.025$	$11.077 - 11.082$	-
	Au	-	$10.902 - 11.081$	-
0 ML	Pd	10.040	-	-
	Pd_3Au	$9.970 - 9.988$	11.173	-
	$PdAu_3$	9.915	$11.062 - 11.090$	-
	Au	-	11.024	-
0.25 ML	Pd	$9.967 - 10.000$	-	1.143
	Pd_3Au	$9.917 - 9.943$	11.160	1.129
	$PdAu_3$	9.880	$11.010 - 11.071$	1.073
	Au	-	$10.973 - 11.041$	1.060
Strained Pd 0.25 ML	$a = 3.85$Å	$9.965 - 9.990$	-	1.134
	$a = 3.95$Å	$9.967 - 10.000$	-	1.143
	$a = 4.05$Å	$9.971 - 10.010$	-	1.148

Effects of hydrogen coverage

Table A.4: *Total energies and adsorption energies as a function of hydrogen coverage.*

		H coverage					
		0	0.25	0.5	0.75	1	1.25
E_{tot}	Pd	−120.63	−124.65	−128.60	−132.53	−136.43	−139.34
	Surface						
	Pd_3Au	−106.50	−110.52	−114.29	−118.00	−121.56	
	Pd_2Au_2	−106.78	−110.61	−114.33	−117.73	−120.96	
	$PdAu_3$	−107.21	−110.70	−114.09	−117.40	−120.29	
	Subsurface						
	Pd_3Au	−106.50	−110.52	−114.29	−118.00	−121.57	
	Pd_2Au_2	−106.62	−110.65	−114.43	−118.08	−121.60	
	$PdAu_3$	−106.65	−110.66	−114.36	−117.97	−121.55	
E_{ad}^{diff}	Pd		−0.63	−0.57	−0.55	−0.52	0.47
	Surface						
	Pd_3Au		−0.65	−0.39	−0.33	−0.18	
	Pd_2Au_2		−0.46	−0.34	−0.02	0.15	
	$PdAu_3$		−0.11	−0.01	0.07	0.49	
	Subsurface						
	Pd_3Au		−0.64	−0.39	−0.33	−0.18	
	Pd_2Au_2		−0.65	−0.40	−0.27	−0.15	
	$PdAu_3$		−0.62	−0.32	−0.23	−0.20	
E_{ad}^{tot}	Pd		−0.63	−1.21	−1.76	−2.28	−1.81
	Surface						
	Pd_3Au		−0.65	−1.03	−1.37	−1.54	
	Pd_2Au_2		−0.46	−0.79	−0.81	−0.66	
	$PdAu_3$		−0.11	−0.12	−0.05	0.44	
	Subsurface						
	Pd_3Au		−0.65	−1.03	−1.37	−1.55	
	Pd_2Au_2		−0.65	−1.05	−1.31	−1.47	
	$PdAu_3$		−0.62	−0.95	−1.17	−1.38	

Diffusion

Adsorption energies along diffusion path

Table A.5: *Adsorption energies along diffusion path.*

		E_{ad} [eV]					
		On surface		Subsurface			
		hcp	fcc	O_{Au}	O_{Bulk}	T	O_{Pd}
Pd	slab	−0.63	−0.59	-	-	−0.26	−0.095
	bulk	-	-	-	-	−0.08	−0.12
Au	slab	0.20	0.25	-	-	-	-
Pd_3Au	slab	−0.059	−0.11	0.19	-	-	−0.21
	bulk	-	-	-	0.13	-	−0.19
$PdAu_3$	slab	–	−0.18	0.15	-	-	−0.04

Barriers and energy differences for diffusion

Table A.6: *Diffusion barriers for Pd and Pd_3Au; slab and bulk.*

		Diffusion barrier [eV]			
		On surface		Subsurface	
		hcp → fcc	fcc → T	O_{Au} →T	T → O_{Pd}
Pd	slab	0.13	0.41	-	0.36
	bulk	-	-	-	0.15
Pd_3Au	slab	0.01	0.45	0.07	-
	bulk	-	-	0.05	-

Table A.7: *Energy differences for Pd and Pd_3Au; slab and bulk.*

		Energy difference [eV]			
		On surface		Subsurface	
		hcp ↔ fcc	fcc ↔ T	O_{Au} ↔ T	T ↔ O_{Pd}
Pd	slab	0.043	0.37	-	0.16
	bulk	-	-	-	0.04
Pd_3Au	slab	0.05	0.26	0.20	0.16
	bulk	-	-	0.14	0.19